Cenozoic Extensional Tectonics in Western and Central Anatolia, Turkey: Introduction

Article *in* Tectonophysics · November 2014

DOI: 10.1016/j.tecto.2014.09.004

3 authors:

Ibrahim Cemen
University of Alabama
107 PUBLICATIONS **1,073** CITATIONS
SEE PROFILE

Cahit Helvacı
Dokuz Eylul University
223 PUBLICATIONS **2,115** CITATIONS
SEE PROFILE

E. Yalçın Ersoy
Dokuz Eylul University
39 PUBLICATIONS **732** CITATIONS
SEE PROFILE

Tectonophysics 635 (2014) 33–58

Contents lists available at ScienceDirect

Tectonophysics

journal homepage: www.elsevier.com/locate/tecto

Tectono-stratigraphy of the Neogene basins in Western Turkey: Implications for tectonic evolution of the Aegean Extended Region

E.Y. Ersoy [a,*], İ. Çemen [b], C. Helvacı [a], Z. Billor [c]

[a] Dokuz Eylül University, Engineering Faculty, Department of Geological Engineering, 35160 İzmir, Turkey
[b] Department of Geological Sciences, The University of Alabama, Tuscaloosa, AL 35487 USA
[c] Department of Geology and Geography, Auburn, AL 36849-5305, USA

ARTICLE INFO

Article history:
Received 2 January 2014
Received in revised form 23 June 2014
Accepted 8 September 2014
Available online 16 September 2014

Keywords:
Aegean-West Anatolia
Neogene basins
Menderes Extensional Metamorphic Complex (MEMC)
Supra-detachment basins
Extensional tectonics

ABSTRACT

The western part of the Aegean region includes several Neogene basins containing volcano-sedimentary successions. The Neogene basins, located along the northern Menderes Extensional Metamorphic Complex (MEMC) were developed during the Miocene as supra-detachment basins. They contain two distinct volcano-sedimentary successions, separated by a regional unconformity. The basins located to the west of the MEMC were developed as strike-slip basins and contain volcanic and sedimentary units getting younger from NE to SW with no remarkable unconformity.

Available paleomagnetic studies in the Aegean Region suggest to us that, the basins to the west of the MEMC were developed in response to southward clockwise rotational roll-back of the Aegean subduction zone. The eastern margin of this rotational deformation is characterized on the surface by a large strike-slip zone, which is known as İzmir–Balıkesir Transfer Zone (İBTZ). The sedimentary successions in the basins along the northern MEMC do not show southward younging and are interpreted to be developed in response to exhumation of the MEMC. During the Pliocene to Quaternary, ~E–W-trending grabens such as the Gediz (Alaşehir), Büyük and Küçük Menderes Grabens were developed in response to tectonic escape accompanying the slab-roll back process. These grabens truncate the MEMC basins. During this time, strike-slip deformation and associated sedimentation continued along the İBTZ.

1. Introduction

The Aegean Extensional Province has a long and complex geological history (Fig. 1). It has experienced several compressional and extensional deformational phases which have been summarized in many papers (e.g., Çemen et al., 2006; Jolivet et al., 2013; Okay and Tüysüz, 1999; Rimmelé et al., 2003; Ring et al., 2010; Şengör and Yılmaz, 1981; van Hinsbergen et al., 2005, 2010a). All researchers agree that the province has experienced a Cenozoic extensional tectonics which is still effective. However, the timing of initiation of the Cenozoic extension has been controversial. Many researchers proposed that the Cenozoic extensional tectonics in the western Anatolian part of the region was initiated in the Middle (e.g., Yılmaz et al., 2000) or earliest Miocene (e.g., Seyitoğlu et al., 1992). Several recent studies, however, proposed that the extension has begun in Late Oligocene in western Anatolia (e.g., Catlos and Çemen; 2005; Çemen et al., 2006; Lips et al., 2001), or in Early Eocene in the Rhodope region (cf., Jolivet and Brun, 2010).

The cause of the Cenozoic extension has also been controversial. The proposed mechanisms of extension include a) post-collisional extension, generated in response to crustal thickening after the collision between the Tauride–Anatolide Platform and the Sakarya Continent (e.g., Seyitoğlu et al., 1992); b) westward escape or lateral extrusion of the Anatolian plate along the North Anatolian and the East Anatolian Fault Zones (Çemen et al., 1999; Şengör and Yılmaz, 1981; Şengör et al., 1985), due to the Eurasian and Arabian plate collision along the Zagros suture zone; c) subduction roll-back and associated back-arc extension (Jolivet and Brun, 2010; Jolivet et al., 2013; Le Pichon and Angelier, 1981; Meulenkamp et al., 1988, 1994; Spakman et al., 1988) and d) a three-stage continuous simple shear extensional model as a result of the mechanisms listed above (Çemen et al., 2006; Gessner et al., 2013).

One of the key areas in the Aegean Extensional Province is the western Anatolia (Figs. 1 and 2) which contains the Menderes Extensional Metamorphic Complex (MEMC) (Bozkurt and Park, 1994; Çemen et al., 2006; Emre, 1996; Işık and Tekeli, 2001; Lips et al., 2001), one of the largest metamorphic core complexes in the world. The MEMC has begun to develop during the Late Oligocene–Early Miocene extensional deformation (e.g., Bozkurt and Park, 1994; Çemen

* Corresponding author. Fax: +90 232 301 73 46.
E-mail address: yalcin.ersoy@deu.edu.tr (E.Y. Ersoy).

http://dx.doi.org/10.1016/j.tecto.2014.09.002
0040-1951/

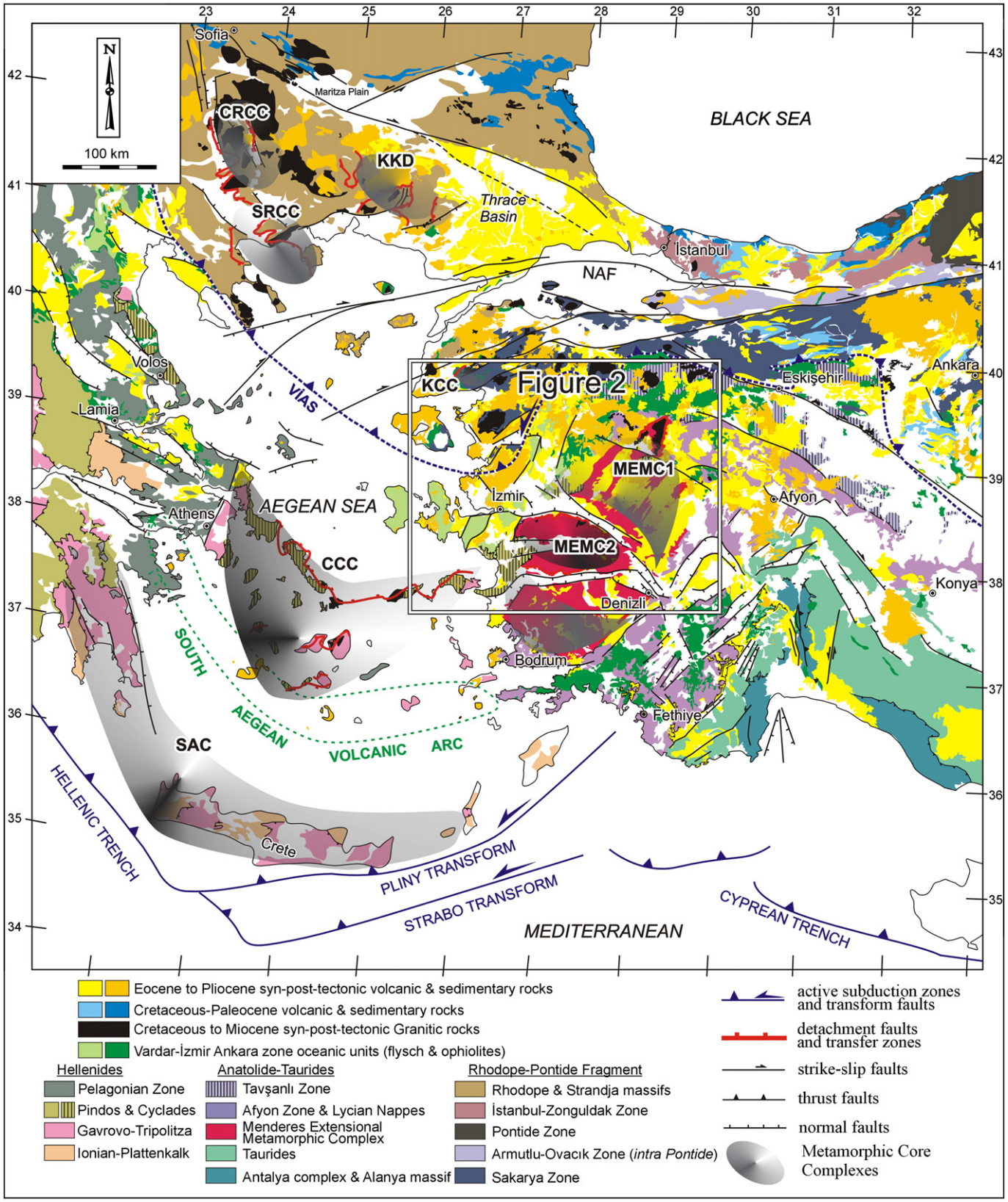

Fig. 1. Tectonostratigraphic units and major tectonic elements of the Aegean Extensional Province (compiled from 1/500,000 scaled geological maps of Greece (IGME) and Turkey (MTA), Okay and Tüysüz, 1999; Ring et al., 2001, 2010; Candan et al., 2005; van Hinsbergen et al., 2005; Ersoy and Palmer, 2013). CRCC: Central Rhodope, SRCC: Southern Rhodope, KCC: Kazdağ, CCC: Cycladic, SAC: South Aegean (Crete) core complexes. KKD: Kesebir–Kardamos Dome. MEMC1 and MEMC2 refer to first- and second-stage development of the Menderes Extensional Metamorphic Complex (MEMC). VİAS: Vardar–İzmir–Ankara suture zone, NAF: North Anatolian Fault Zone.

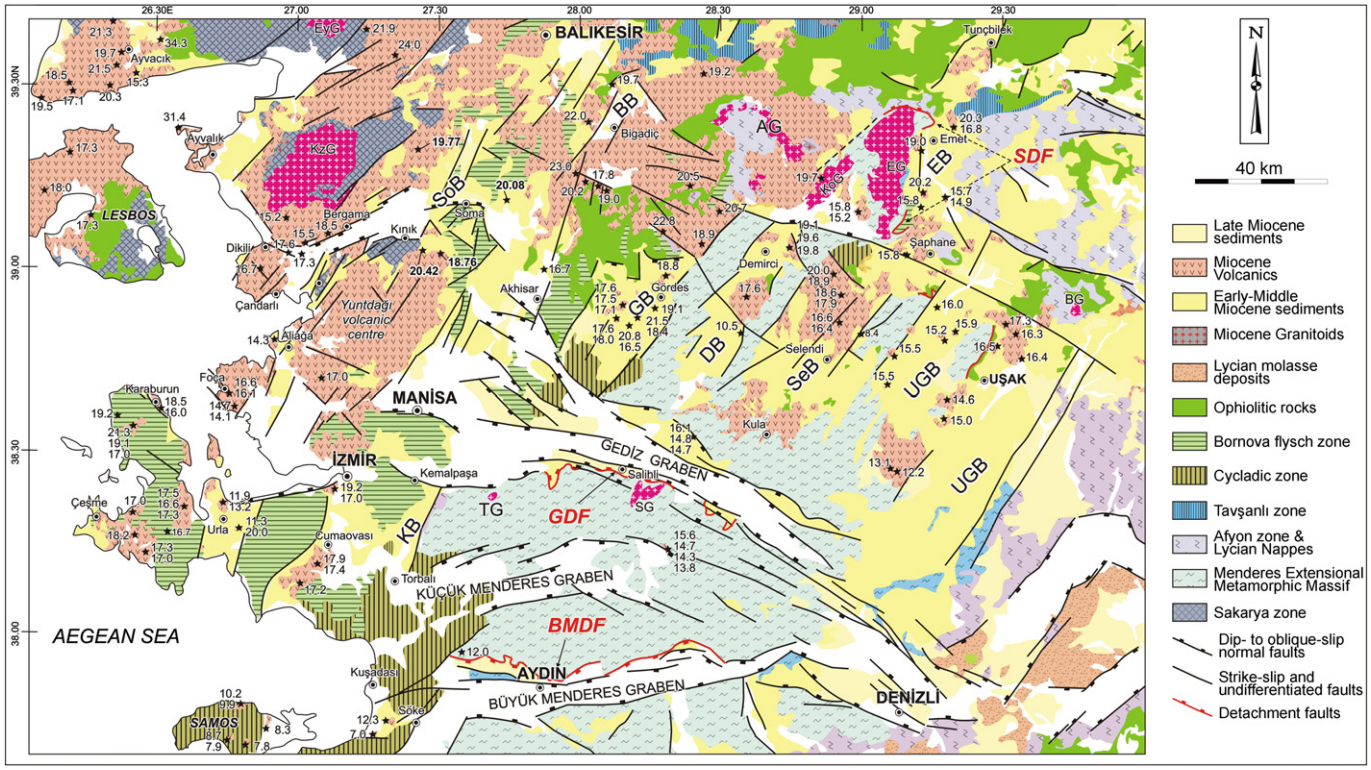

Fig. 2. Geological map of the western Anatolia showing the distribution of the Neogene basins, radiometric ages of the volcanic intercalations in the Neogene sediments and major structures (modified from 1/500,000 scaled geological map of Turkey (MTA); and studies cited in the text). Abbreviations for granitoids: EyG: Eybek, KzG: Kozak, AG: Alaçamdağ, Kog, Koyunoba, EG: Eğrigöz, BG: Baklan, TG: Turgutlu and SG: Salihli granitoids. Abbreviations for basins: KB: Kemalpaşa Basin, SoB: Soma Basin, GB: Gördes Basin, DB: Demirci Basin, SeB: Selendi Basin, UGB: Uşak–Güre Basin, EB: Emet Basin. Abbreviations for detachments: GDF: Gediz (Alaşehir) Detachment Fault, SDF: Simav Detachment Fault, BMDF: Büyük Menderes Detachment Fault. See references in Tables 1, 2 and 3 for age data.

et al., 2006; Glodny and Hetzel, 2007; Hetzel et al., 1995; Işık and Tekeli, 2001; Işık et al., 2004) and occurred in poly-phase deformation.

The MEMC is bounded by NE–SW trending Miocene strike-slip faults (Figs. 1 and 2) along its eastern and western margin edges, implying that the exhumation of the MEMC has not occurred simply with domal uplift along crustal-scale low-angle extensional detachment faults, rather it was exhumed along the interaction of both low-angle detachments and high-angle strike-slip faults (Çemen et al., 2006; Ersoy et al., 2011; Sözbilir et al., 2011). The NE–SW trending strike-slip faulting along the western part of the MEMC is known as the İzmir–Balıkesir Transfer Zone (İBTZ; Sözbilir et al., 2003; Erkül et al., 2005; Kaya et al., 2007; Uzel and Sözbilir, 2008; Ersoy et al., 2011; Gessner et al., 2013), along which several Miocene to Recent transtensional areas and basins were developed. The NE–SW trending Southwestern Anatolian Shear Zone (Çemen et al., 2006; Karaoğlu and Helvacı, 2012), bounds the eastern edge of the MEMC and contains several oblique-slip faults and associated extensional basins. These areas, which are still actively being deformed, are also important in the extensional history of the region.

The main objectives of this paper are 1) to discuss available stratigraphic, sedimentological and structural data from the Miocene basins on and around the MEMC together with our data from these basins; 2) to evaluate implications of our new Ar/Ar age data together with other available radiometric ages; and 3) to propose a new model for the evolution of the Cenozoic extensional basins in western Turkey.

2. Regional geology

The western Anatolia, Turkey, is situated in the Alpine–Himalayan orogenic belt (e.g., Hetzel et al., 1995; Jolivet et al., 2013; Şengör and Yılmaz, 1981). In this region Laurasia-affiliated Rhodope–Pontide fragment (Ricou et al., 1998), including Rhodope–Strandja massifs, Pontides, İstanbul–Zoguldak, Armutlu–Ayvacık and Sakarya zones to the north, collided with the Gondwana-affiliated microcontinents along the northern branch of the Neo-Tethys (Fig. 1; Şengör and Yılmaz, 1981; Okay and Tüysüz, 1999; Yiğitbaş et al., 1999; Ring et al., 2010). Gondwana-affiliated micro-continents to the south of the Vardar–İzmir–Ankara Suture Zone (VİASZ) are Anatolide–Tauride block (ATB) in western Anatolia and the Pelagonia and Apulia zones in continental Greece and in the Aegean islands. The collision along the VİASZ formed the late Cretaceous high-pressure belt of the Tavşanlı and Afyon zones (Candan et al., 2005; Okay and Tüysüz, 1999; Plunder et al., 2013). During Eocene–Oligocene, the Lycian nappes were transported from north to south as part of Afyon Zone and formed a polymetamorphic tectonic unit of the ATB. This time also marks the formation of the high-pressure Cycladic zone in the central Aegean (Ring et al., 2010 and references therein).

It has been suggested that the Cenozoic extensional tectonics in the Aegean was initiated as early as the Eocene (~45 Ma) by slab-roll back processes which produced the Rhodope Metamorphic Core Complex in the northernmost Aegean (Brun and Faccenna, 2008; Brun and Sokoutis, 2012; Dinter and Royden, 1993). The Cenozoic extensional tectonics and related core complex formation migrated to the south with time, and during the Late Oligocene to Middle Miocene times, Kazdağ, Cycladic and Menderes Extensional Core Complexes formed.

The northern flank of the MEMC was exhumed in three main stages: (1) latest Oligocene–Early Miocene detachment faulting along the Simav Detachment Fault (SDF; Işık and Tekeli, 2001; Işık et al., 2000), (2) Middle Miocene detachment faulting along Gediz (Alaşehir) Detachment Fault (GDF; e.g., Emre, 1996; Seyitoglu et al., 2002) and Büyük Menderes Detachment Fault (BMDF; e.g., Bozkurt, 2000; Çemen et al., 2006; Gürer et al., 2009) and (3) Pliocene–Quaternary

Table 1
Radiometric age data from the Simav and Gediz detachment faults and syn-extensional Eğrigöz, Koyunoba, Salihli and Turgutlı granitoids.

Analyzed rock	Age	Material, method and reference	Interpretation
Simav Detachment Fault			
Mylonitic gneisses	22.86 ± 0.47 Ma	(Muscovite, Ar/Ar) (Işık et al., 2004)	Timing of ductile deformation
Orthogneisses	29.60 ± 1.10 Ma	(Monazite, Th–Pb) (Catlos and Çemen, 2005)	
Orthogneisses	27.90 ± 1.00 Ma	(Monazite, Th–Pb) (Catlos and Çemen, 2005)	
Fault zone rock	31.20 ± 1.80 Ma	(Muscovite, Rb/Sr) (Bozkurt et al., 2011)	
Fault zone rock	30.10 ± 1.00 Ma	(Muscovite, Rb/Sr) (Bozkurt et al., 2011)	
Fault zone rock	28.30 ± 1.60 Ma	(Muscovite, Rb/Sr) (Bozkurt et al., 2011)	
Fault zone rock	29.50 ± 1.40 Ma	(Muscovite, Rb/Sr) (Bozkurt et al., 2011)	
Fault zone rock	28.50 ± 0.80 Ma	(Muscovite, Rb/Sr) (Bozkurt et al., 2011)	
Fault zone rock	16.70 ± 0.60 Ma	(Biotite, Rb/Sr) (Bozkurt et al., 2011)	
Fault zone rock	15.10 ± 0.60 Ma	(Biotite, Rb/Sr) (Bozkurt et al., 2011)	
Fault zone rock	13.10 ± 3.60 Ma	(Biotite, Rb/Sr) (Bozkurt et al., 2011)	
Fault zone rock	13.60 ± 0.40 Ma	(Biotite, Rb/Sr) (Bozkurt et al., 2011)	
Fault zone rock	10.70 ± 0.20 Ma	(Biotite, Rb/Sr) (Bozkurt et al., 2011)	
Orthogneise	45.70 ± 0.60 Ma	(Muscovite, Rb/Sr) (Bozkurt et al., 2011)	
Orthogneise	18.20 ± 0.20 Ma	(Biotite, Rb/Sr) (Bozkurt et al., 2011)	
Eğrigöz granitoid	20.00 ± 0.70 Ma	(Biotite, K/Ar) (Bingöl et al., 1982)	Cooling/crystallization age for the granitoid
	20.40 ± 0.60 Ma	(Biotite, K/Ar) (Bingöl et al., 1982)	Crystallization age for the granitoid
	20.19 ± 0.28 Ma	(Biotite, Ar/Ar) (Işık et al., 2004)	Crystallization age for the granitoid
	19.00 ± 0.10 Ma	(Hornblende, Ar/Ar) (Altunkaynak et al., 2012)	Cooling age for the granitoid
	18.90 ± 0.10 Ma	(Biotite, Ar/Ar) (Altunkaynak et al., 2012)	Cooling age for the granitoid
	18.77 ± 0.19 Ma	(Biotite, Rb/Sr) (Hasözbek et al., 2010)	Cooling age for the granitoid
	19.48 ± 0.29 Ma	(Zircon, U–Pb) (Altunkaynak et al., 2012)	Emplacement age for the granitoid
	19.40 ± 4.40 Ma	(Zircon, U–Pb) (Hasözbek et al., 2010)	Crystallization age for the granitoid
	20.70 ± 0.60 Ma	(Zircon, U–Pb) (Ring and Collins, 2005)	Emplacement age for the granitoid
Koyunoba granitoid	21.00 ± 0.20 Ma	(Zircon, U–Pb) (Ring and Collins, 2005)	Emplacement age for the granitoid
	21.70 ± 1.00 Ma	(Zircon, U–Pb) (Hasözbek et al., 2010)	Crystallization age for the granitoid
Gediz Detachment Fault			
Cataclasite	6.56 ± 2.46 Ma	(Muscovite, Ar/Ar) (Lips et al., 2001)	(Semi)ductile deformation related to reactivation
	6.70 ± 1.10 Ma	(Muscovite, Ar/Ar) (Lips et al., 2001)	
Salihli granitoid	17.90 ± 1.00 Ma	(Hornblende, Ar/Ar) (Hetzel et al., 1995)	Minimum intrusion age for the granitoid
	12.20 ± 0.40 Ma	(Biotite, Ar/Ar) (Hetzel et al., 1995)	Cooling age for the granitoid (extension lasted)
	12.60 ± 0.40 Ma	(Biotite, Ar/Ar) (Hetzel et al., 1995)	Cooling age for the granitoid (extension lasted)
	15.00 ± 0.30 Ma	(Allanite, Th–Pb) (Glodny and Hetzel, 2007)	Crystallization age of the granitoid
	15.00 ± 2.80 Ma	(Monazite, Th–Pb) (Catlos et al., 2008)	Crystallization age of the granitoid
Turgutlu granitoid	13.10 ± 0.20 Ma	(Biotite, Ar/Ar) (Hetzel et al., 1995)	Cooling age for the granitoid (extension lasted)
	13.30 ± 0.30 Ma	(Biotite, Ar/Ar) (Hetzel et al., 1995)	Cooling age for the granitoid (extension lasted)
	16.10 ± 0.20 Ma	(Monazite, U–Pb) (Glodny and Hetzel, 2007)	Crystallization age of the granitoid
	15.00 ± 1.7 Ma	(Monazite, U–Pb) (Catlos et al., 2008)	Crystallization age of the granitoid

high-angle normal faulting, cutting the older structures throughout the western Anatolia (Yılmaz et al., 2000). Each of these stages is responsible for deformation, basin formation, sedimentation and extensive volcanic activity in the upper plate.

The first stage of extension has occurred along the Simav Detachment Fault (SDF). Muscovite Ar/Ar age of 22.86 ± 0.47 Ma (Işık et al., 2004; Table 1) is interpreted as the timing of ductile deformation along the SDF. Zircon and apatite fission track ages from the footwall of the SDF also show that the deformation was active between ~25 and 19 Ma (Thomson and Ring, 2006). Th–Pb monazite ages also indicate an Oligocene age for the deformation in the northern part of the MEMC (Catlos and Çemen, 2005; Çemen et al., 2006). Bozkurt et al. (2011) also reported Oligocene age of 29.5 ± 1.4 from the SDF. These radiometric age determinations suggest that the Cenozoic extensional deformation in the northern MECM (along the SDF) has begun during the Late Oligocene. Radiometric ages from the syn-kinematic Eğrigöz and Koyunoba granitoids indicate that the plutons emplaced, crystallized and cooled between 21.7 and 18.77 Ma ago (Table 1). Several supra-detachment basins in the upper plate, such as Demirci, Selendi and Uşak–Güre basins are located in the northern MECM (e.g., Çemen et al., 2006; Ersoy et al., 2011; Purvis et al., 2005). However, there is no supradetachment basin in the southern MEMC. This suggests that the first-stage exhumation of the MEMC has occurred asymmetrically (e.g., Seyitoğlu et al., 2004).

The second stage of the Cenozoic extension in the MEMC occurred in its central parts, along the north-dipping Gediz (Alaşehir) Detachment Fault (GDF) and south-dipping Büyük Menderes Detachment Fault (BMDF). These faults have also controlled the basins in the upper plate (e.g., Çemen et al., 2006; Çiftçi and Bozkurt, 2009; Öner and Dilek, 2013; Şen and Seyitoğlu, 2009; Sözbilir, 2002). The footwall of the GDF was intruded by the Salihli and Turgutlu granitoids (e.g., Hetzel et al., 1995; Glodny and Hetzel, 2007; Catlos et al., 2010). Intrusion ages of these granitoids are reported generally between 16 and 15 Ma (Table 1). Young ages from the cataclasites of the GDF are generally interpreted as the reactivation (Catlos and Çemen, 2005; Lips et al., 2001). The episodic exhumation of the MEMC was also accompanied by Miocene to Recent NE–SW-trending strike-slip faulting along its western margin (Ersoy et al., 2011) known as the İzmir–Balıkesir Transfer zone (İBTZ; Sözbilir et al., 2003; Erkül et al., 2005; Uzel and Sözbilir, 2008; Ersoy et al., 2011; Uzel et al., 2013; Karaoğlu, 2014). Complex deformation along the İBTZ also resulted in basin formation and volcanic activity (Ersoy et al., 2010b).

3. Stratigraphy of the Neogene basins

In this section, stratigraphy of the Neogene sedimentary units and their relations to the volcanic rocks will be reviewed with the new field and radiometric data. First, we will describe the stratigraphy of the basins located along the western margin of the Menderes Extensional Metamorphic Complex (MEMC), from north to south by referring to their geographic locations. Second, we will describe the stratigraphy and structural features of the NE–SW-trending Neogene basins developed on the northern MEMC.

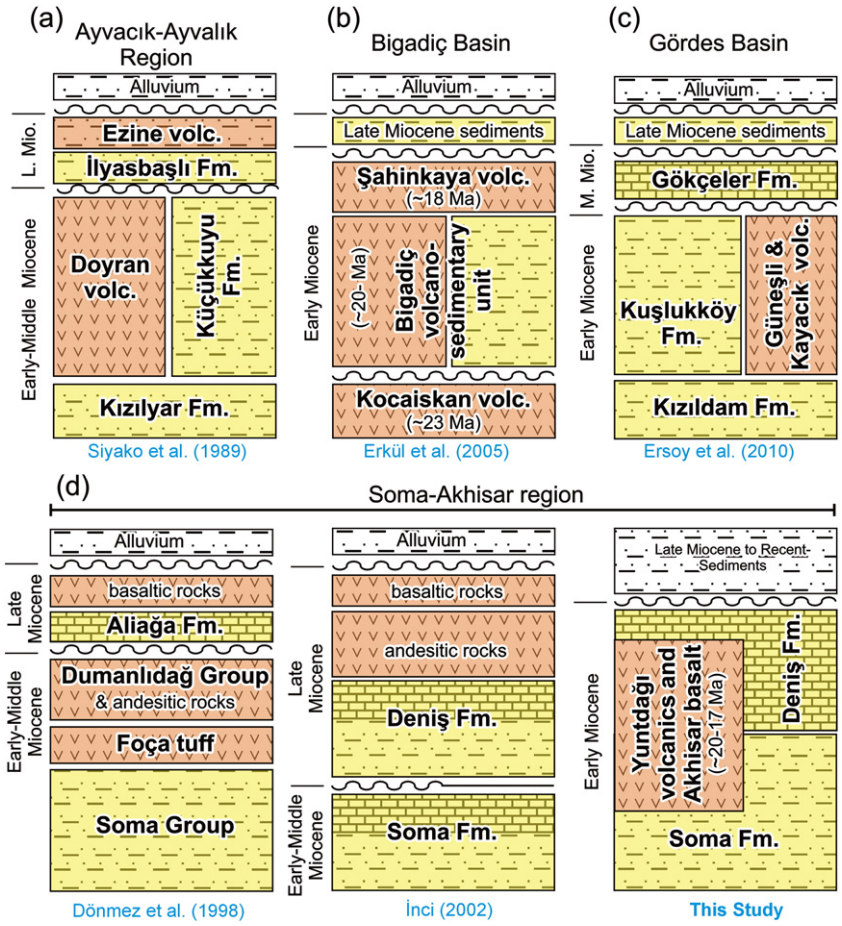

Fig. 3. Comparison of Miocene stratigraphy of the Ayvacık–Ayvalık Region (a), Bigadiç Basin (b), Gördes Basin (c) and Soma–Akhisar Region (d).

3.1. Neogene basins along the western margin of the (MEMC)

3.1.1. Ayvacık–Ayvalık area and surrounding region

In the Ayvacık–Ayvalık area (lat: 39°.30′; long: 26°.30′–27°.00′; Fig. 2), the Cenozoic sedimentary succession begins with conglomerates of Kızılyar formation, and continues upward with Küçükkuyu formation. Both formations are interfingered with felsic rocks of the Doyran volcanics (Siyako et al., 1989; Fig. 3a). Felsic volcanic rocks overlying Kızılyar and Küçükkuyu formations have yielded 21.3 ± 0.3–19.7 ± 0.3 Ma K–Ar ages (Aldanmaz et al., 2000; Table 2). This suggests an Early Miocene age for the sedimentary units underlying the felsic volcanic rocks.

The sedimentary units around the town of Ayvalık are called as Ballıca and Soma Formations (Akyürek and Soysal, 1983). Ercan et al. (1985) reported 31.4 ± 0.4 Ma K–Ar age from the Alibey volcanics in the vicinity of Ayvalık, and the felsic volcanic rocks of Oligocene age occur to the north of the Ayvacık–Ayvalık Region (Fig. 2). There are also Late Miocene sediments and volcanic rocks in the Ayvalık–Ayvacık Region (Aldanmaz et al., 2000; Siyako et al., 1989). In the same latitudes, but to the east of the Ayvacık–Ayvalık Region, borate-bearing Neogene sedimentary units of the Bigadiç Basin rest unconformably on the andesitic volcanic rocks of 23 ± 2.80 Ma (K–Ar) (Erkül et al., 2005). The volcanic intercalations in the borate-bearing fluvio-lacustrine sediments of the Bigadiç Basin yielded radiometric ages between 20.6 ± 0.7 and 18.3 ± 0.2 Ma (Erkül et al., 2005; Helvacı, 1995) (Fig. 3b; Table 2). These units are overlain by the Late Miocene–Pliocene continental deposits with no volcanic intercalations.

3.1.2. Soma–Akhisar and Dikili–Bergama areas and surrounding region

In this region, the Gördes Basin is located to the south of the Bigadiç Basin (Fig. 2), between the ophiolitic mélange units of the İzmir–Ankara zone and the metamorphic rocks of the Menderes Extensional Metamorphic Complex (MEMC) (lat: ~39°.00′; long: 27°.00′–28°.00′; Fig. 2). The basin-fill starts with the conglomerates of the Kızıldam formation of alluvial-fan origin (Fig. 3c). This unit deposited along the basin-margin, grades laterally and vertically into the fluvial rocks of the Kuşlukköy Formation which is interbedded with, and also cut by the felsic volcanic rocks of the Güneşli volcanics in the northern part of the basin (Ersoy et al., 2011). The radiometric ages from these volcanic rocks vary in a range of 22.8 ± 1.0–17.0 ± 0.4 Ma (K/Ar and Ar/Ar) (Çoban et al., 2012; Ersoy et al., 2012; Purvis et al., 2005; Seyitoğlu and Scott, 1994; Seyitoğlu et al., 1992) and give an Early Miocene age for the deposition of the Kızıldam formation (Table 2). The Kuşlukköy formation is also interbedded with, and also cut by the dacitic–rhyolitic volcanic rocks of the Kayacık volcanics in the center of the basin, which yielded 21.71 ± 0.04 to 16.03 ± 0.50 Ma K/Ar and Ar/Ar radiometric ages (Ersoy et al., 2011; Seyitoğlu and Scott, 1994; Seyitoğlu et al., 1992). The younger ages among these data are obtained from the volcanic necks in the center of the basin (Purvis et al., 2005; Seyitoğlu et al., 1992). In the Gördes Basin, relatively undeformed fluvio-lacustrine sediments with small outcrops unconformably overly the Early Miocene sedimentary units (Gökçeler Formation). There is no age data from these units, but they may be correlative with the late Early to Middle Miocene sediments in the adjacent basins (Ersoy et al., 2011). These sedimentary units can also be correlated with the upper sedimentary units in the Soma–Akhisar Region (see below).

Table 2
Radiometric age data from the volcanic rocks along the western part of the Menderes Extensional Metamorphic Complex. n.a.: not available data.

Ayvacık–Ayvalık Region			
Kızıltepe volc. unit	EA-67	Trachyandesite	21.30 ± 0.30 (K–Ar) (Aldanmaz et al., 2000)
Akçapınar volc. unit	EA-151	Andesite	19.70 ± 0.30 (K–Ar) (Aldanmaz et al., 2000)
Ballıca volc. unit	EA-278	Latite	20.90 ± 0.50 (K–Ar) (Aldanmaz et al., 2000)
Kovaclı dikes	EA-418	B. tarchyand.	19.70 ± 0.30 (K–Ar) (Aldanmaz et al., 2000)
Behram andesite	EA-37	Trachyandesite	20.30 ± 0.60 (K–Ar) (Aldanmaz et al., 2000)
Koyunevi Ignimbrite	EA-77	Rhyolitic	20.50 ± 0.50 (K–Ar) (Aldanmaz et al., 2000)
Bigadiç Basin			
Kocaiskan volcanics	F-110	Andesite	23.00 ± 2.80 (biotite, K–Ar) (Erkül et al., 2005)
Gölcük Basalt	F-199	Shoshonite	19.70 ± 0.40 (groundmass, Ar–Ar) (Erkül et al., 2005)
	F-199	Shoshonite	20.50 ± 0.10 (groundmass, Ar–Ar) (Erkül et al., 2005)
Sındırgı volcanics	F-194	Rhyolite	20.20 ± 0.50 (biotite, Ar–Ar) (Erkül et al., 2005)
	F-197	Dacite	20.30 ± 0.30 (biotite, Ar–Ar) (Erkül et al., 2005)
Çamköy basalt	B-6	Basalt	18.30 ± 0.20 (feldspar, K–Ar) (Helvacı, 1995)
Şahinkaya volcanics	F-195	B. andesite	17.80 ± 0.40 (hornblende, K–Ar) (Erkül et al., 2005)
Kayırlar volcanics	F-214	Latite	20.60 ± 0.70 (biotite, K–Ar) (Erkül et al., 2005)
Dikili–Bergama Region			
Nebiler volcanics	EA-143	B. andesite	15.20 ± 0.40 (K–Ar) (Aldanmaz et al., 2000)
Eğrigöl andesite	EA-314	Andesite	15.50 ± 0.30 (K–Ar) (Aldanmaz et al., 2000)
Dikili volcanics	TD-93	Trachyte	16.7 (±3.5%) (biotite, K–Ar) (Borsi et al., 1972)
Dikili volcanics	TD-110	Andesite	17.6 (±3.5%) (biotite, K–Ar) (Borsi et al., 1972)
Dikili volcanics	TD-112	Dacite	17.3 (±3.5%) (biotite, K–Ar) (Borsi et al., 1972)
Bergama	TD107	n.a.	18.5 (±3.5%) (biotite, K–Ar) (Borsi et al., 1972)
Soma–Akhisar Region			
Around Göçbeyli	128	Trachyte	19.77 ± 0.03 (biotite, Ar–Ar) (this study)
Yuntdağ volcanics	116	Dacite	18.76 ± 0.05 (biotite, Ar–Ar) (this study)
	115	Andesite	20.42 ± 0.12 (whole rock, Ar–Ar) (this study)
	S-906	Andesite	17.00 ± 0.30 (whole rock, Rb–Sr) (Ercan et al., 1996)
Dededağ volcanics	915	Andesite	20.08 ± 0.12 (whole rock, Ar–Ar) (this study)
Adilköy basalt	124 (AdB)	Basalt	20.40 ± 0.18? (whole rock, Ar–Ar) (this study)
	911 (AdB)	Basalt	20.72 ± 0.10 (whole rock, Ar–Ar) (this study)
Akhisar basalt	ÖD-40 (AkB)	UK-latite	16.90 ± 0.30 (K–Ar) (Ercan et al., 1996)
	IZ-6 (AkB)	UK-latite	16.72 ± 0.15 (groundmass, Ar–Ar) (Innocenti et al., 2005)
Gördes Basin			
Kayacık volcanics	LB-1	Dacite	16.90 ± 0.50 (biotite, K–Ar) (Seyitoğlu et al., 1992)
	LP-1	Dacite	17.10 ± 0.60 (biotite, K–Ar) (Seyitoğlu et al., 1992)
	KRC	Rhyolite	17.20 ± 0.50 (biotite, K–Ar) (Seyitoğlu et al., 1992)
	KD	Dacite	17.50 ± 0.50 (biotite, K–Ar) (Seyitoğlu et al., 1992)
	TSB	Rhyolite	18.10 ± 0.50 (biotite, K–Ar) (Seyitoğlu et al., 1992)
	TSB	Rhyolite	17.90 ± 0.50 (biotite, K–Ar) (Seyitoğlu et al., 1992)
	BK	Rhyolite	18.40 ± 0.80 (biotite, K–Ar) (Seyitoğlu et al., 1992)
	BK	Rhyolite	18.40 ± 0.80 (biotite, K–Ar) (Seyitoğlu et al., 1992)
	AZ	Rhyolite	17.00 ± 0.80 (biotite, K–Ar) (Seyitoğlu et al., 1992)
	YK	Rhyolite	16.05 ± 0.50 (biotite, K–Ar) (Seyitoğlu et al., 1992)
	YK	Rhyolite	16.03 ± 0.50 (biotite, K–Ar) (Seyitoğlu et al., 1992)
	S1/36	Rhyodacite	17.60 ± 0.10 (biotite, Ar/Ar) (Purvis et al., 2005)
	S1/38	Rhyodacite	17.62 ± 0.07 (biotite, Ar/Ar) (Purvis et al., 2005)
	S2/5	Rhyodacite	20.86 ± 0.08 (feldspar, Ar/Ar) (Purvis et al., 2005)
	S2/5	Rhyodacite	20.45 ± 0.38 (feldspar, Ar/Ar) (Purvis et al., 2005)
	S2/11	Acidic tuff	21.71 ± 0.04 (biotite, Ar/Ar) (Purvis et al., 2005)
	S2/11	Acidic tuff	20.49 ± 0.09 (biotite, Ar/Ar) (Purvis et al., 2005)
	S2/4	Acidic tuff	19.16 ± 0.09 (biotite, Ar/Ar) (Purvis et al., 2005)
Güneşli volcanics	S2/68	Acidic tuff	17.04 ± 0.35 (biotite, Ar/Ar) (Purvis et al., 2005)
	S2/68	Acidic tuff	18.78 ± 0.30 (biotite, Ar/Ar) (Purvis et al., 2005)
	861	Rhyolite	18.91 ± 0.03 (sanidine, Ar/Ar) (Ersoy et al., 2012)
	861	Rhyolite	18.76 ± 0.09 (sanidine, Ar/Ar) (Ersoy et al., 2012)
	D-63	Dacite	20.70 ± 0.50 (mica, K–Ar) (Çoban et al., 2012)
	12	Andesite	22.80 ± 1.00 (amphibole, K–Ar) (Çoban et al., 2012)
Foça–Aliağa–İzmir Region			
Foça mafic rocks	ÖD-39	K-trachybas.	14.30 ± 0.30 (whole rock, K–Ar) (Ercan et al., 1996)
	SF-11	Phonolite	14.12 ± 0.95 (plagioclase, Ar–Ar) (Altunkaynak et al., 2010)
	SF-17	Trachyte	14.60 ± 3.30 (biotite, Ar–Ar) (Altunkaynak et al., 2010)
	SF-18	Trachyte	14.73 ± 0.57 (plagioclase, Ar–Ar) (Altunkaynak et al., 2010)
Foça felsic rocks	SF-27	Rhyolite	16.63 ± 0.84 (biotite, Ar–Ar) (Altunkaynak et al., 2010)
	SF-39	Benmoerite	16.50 ± 1.40 (biotite, Ar–Ar) (Altunkaynak et al., 2010)
	SF-31	Rhyolite	16.10 ± 0.69 (biotite, Ar–Ar) (Altunkaynak et al., 2010)
	SF-33	Rhyolite	16.50 ± 1.10 (biotite, Ar–Ar) (Altunkaynak et al., 2010)
	SF-33	Rhyolite	16.22 ± 0.37 (plagioclase, Ar–Ar) (Altunkaynak et al., 2010)
Around İzmir	KAD	Andesite	19.2 (±3.5%) (amphibole, K–Ar) (Borsi et al., 1972)
Karaburun Peninsula and surroundings			
Cumaovası volcanics	TD83	Rhyolite	12.50 (feldspar Rb–Sr) (Borsi et al., 1972)
	CV-4	Dacite	17.20 ± 0.50 (whole rock, K–Ar) (Karacık et al., 2013)
	CV-28	Dacite	17.20 ± 0.50 (whole rock, K–Ar) (Karacık et al., 2013)

Table 2 (*continued*)

Karaburun Peninsula and surroundings			
	CV-17	Rhyolite	17.60 ± 0.50 (whole rock, K–Ar) (Karacık et al., 2013)
	CV-57	Rhyolite	17.90 ± 0.60 (whole rock, K–Ar) (Karacık et al., 2013)
	CV-65	Rhyolite	17.40 ± 0.60 (whole rock, K–Ar) (Karacık et al., 2013)
Karaburun basalt	KB-2-YT	Basalt	18.50 ± 3.10 (matrix, K–Ar) (Türkecan et al., 1998)
	KB-8-YT	Basalt	16.00 ± 0.70 (matrix, K–Ar) (Türkecan et al., 1998)
Kocadağ volcanics	FK-1	Dacite	17.50 ± 0.10 (whole rock, Ar–Ar) (Helvacı et al., 2009)
	K-54	Dacite	17.30 (±3.5%) (matrix, K–Ar) (Borsi et al., 1972)
	K-58	Rhyolite	16.60 (±3.5%) matrix, K–Ar) (Borsi et al., 1972)
Armağandağ volc.	HS-294	Andesite	17.30 ± 0.10 (whole rock, Ar–Ar) (Helvacı et al., 2009)
	K-64	Andesite	18.20 (±3.5%) (whole rock, K–Ar) (Borsi et al., 1972)
	K-94	Andesite	17.00 (±3.5%) (biotite, K–Ar) (Borsi et al., 1972)
Yaylaköy volcanics	K-87	Andesite	21.3 (±3.5%) (whole rock, K–Ar) (Borsi et al., 1972)
	K-83	Andesite	19.2 (±3.5%) (whole rock, K–Ar) (Borsi et al., 1972)
	FK-3	Andesite	17.00 ± 0.40 (groundmass, Ar–Ar) (Helvacı et al., 2009)
Urla volcanics	K75	Trachyte	11.9 (±3.5%) (whole rock, K–Ar) (Borsi et al., 1972)
	KV-39	Trachyte	13.20 ± 0.30 (sanidine, K–Ar) (Karacık et al., 2013)
Ovacık basalt	T-92	Hawaiite	11.3 (±3.5%) (whole rock, K–Ar) (Borsi et al., 1972)
	KV-17	Basalt	20.00 ± 1.10 (whole rock, K–Ar) (Karacık et al., 2013)
Torbalı/Kocaçay Basin			
Tuff layer	KT-01	Pyroclastic	13.40 ± 0.10 Ma (biotite, Ar–Ar) (Sözbilir et al. 2011)
Samos–Söke Region			
Samos Island	11	Rhyolite	10.20 ± 0.30 (whole rock, K–Ar) (Pe-Piper and Piper, 2007)
	35	Trachyte	9.90 ± 0.30 (whole rock, K–Ar) (Pe-Piper and Piper, 2007)
	77	Rhyolite	8.70 ± 0.40 (whole rock, K–Ar) (Pe-Piper and Piper, 2007)
	9	Basalt	8.30 ± 0.40 (whole rock, K–Ar) (Pe-Piper and Piper, 2007)
	43	Basalt	7.80 ± 0.50 (whole rock, K–Ar) (Pe-Piper and Piper, 2007)
	29	Basalt	7.90 ± 0.30 (whole rock, K–Ar) (Pe-Piper and Piper, 2007)
Hisartepe volcanics (Söke Region)	SH-02	Latite	12.31 ± 0.09 (groundmass, Ar–Ar) (Sümer et al., 2013)
	22	Latite	6.99 ± 0.22 (whole rock, K–Ar) (Ercan et al., 1985)

To the west of the Gördes Basin, lies the coal-bearing Soma Basin of the Soma–Akhisar area, where the Cenozoic sedimentary succession begins with ephemeral lacustrine and fan-delta deposits and grades into fluvial and shallow lacustrine sediments of the Soma Formation (Dönmez et al., 1998; İnci, 1998, 2002; Fig. 3d). These units are in turn overlain conformably by fine-grained fluvial sediments, lacustrine carbonates and andesitic volcanic rocks of the Yuntdağ volcanics of the Deniş Formation. The Soma Formation is reported to be Early–Middle Miocene in age, and the Deniş Formation is Late Miocene (İnci, 2002). However, Akgün et al. (2007) reported that the age of the coal bearing sediments should be Early Miocene on palynologic data.

Our new Ar/Ar radiometric ages from the volcanic rocks in the Soma Basin and its vicinity, especially from the volcanic rocks directly overlying the Deniş Formation (Fig. 2) are in the range of 20.42 ± 0.12–18.76 ± 0.05 Ma (Table 2). Black-colored andesites (one of the basaltic extrusions of İnci, 1998, 2002), overlying the Deniş Formation to the SE of Kınık and N of Bayat villages yielded 20.42 ± 0.12 and 20.08 ± 0.12 Ma ages, respectively (Fig. 9).

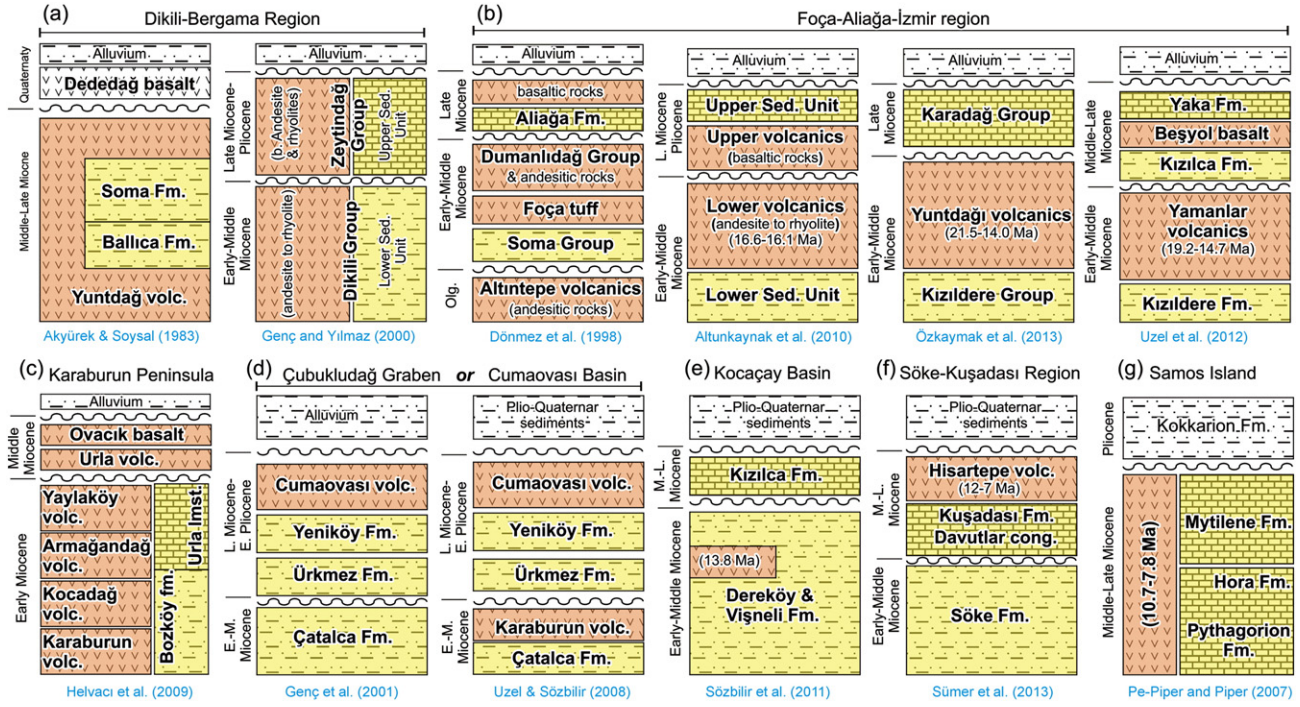

Fig. 4. Comparison of Miocene stratigraphy of the Dikili–Bergama Region (a), Foça–Aliağa–İzmir Region (b), Karaburun Peninsula (c), Çubukludağ Graben or Cumaovası Basin (d), Kocaçay Basin (e), Söke–Kuşadası Region (f) and Samos Island (g).

Similarly, andesites and dacites overlying the Deniş Formation to the farther SE of Kınık and to the N of Göçbeyli yielded 18.76 ± 0.05 and 19.77 ± 0.03 Ma, respectively. These ages suggest that coal-bearing sedimentary succession of the Soma Basin may be deposited before Burdigalian.

Along the road from Akhisar to Gördes, fluvio-lacustrine sediments are conformably overlain by mafic lavas of Akhisar basalt which yielded 16.72 ± 0.15 (Ar/Ar) and 16.90 ± 0.30 Ma (K/Ar) radiometric ages (Ercan et al., 1996; Innocenti et al., 2005; Table 2). These age data indicate that the upper sedimentary units around the Akhisar region are late Early Miocene in age.

To the south of the Ayvacık–Ayvalık Region, around Dikili–Bergama (Figs. 2 and 4a), the Neogene stratigraphy is characterized by two volcano-sedimentary groups: Dikili and Zeytindağ (also known as Çandarlı) groups (Karacık et al., 2007; Yılmaz et al., 2000). The base of the Dikili group is made up of conglomerates of alluvial-fan origin (Akyürek and Soysal, 1983; Kaya, 1981), and siltstones, mudstones and laminated bituminous shales of fluvio-lacustrine origin (Akyürek and Soysal, 1983) (Fig. 4a). Radiometric age data from the volcanic intercalations in the Dikili Group are in the range of 18.5–16.7 Ma (Table 2), indicating a late Early Miocene age for the lower sedimentary unit. The Dikili group likely corresponds to the Early Miocene volcano-sedimentary units in the Ayvacık–Ayvalık Region described above, with slightly younger ages. The sedimentary rocks of the Zeytindağ Group, which are relatively undeformed with respect to the Dikili Group (Genç and Yılmaz, 2000; Karacık et al., 2007), is composed of alluvial fan deposits (Yılmaz et al., 2000), and sandstones, siltstones, mudstones, marls and white lacustrine limestones (Yılmaz et al., 2000). These local sedimentary units with small outcrops overlie the Dikili group and are intercalated with volcanic rocks of 15.50 ± 0.30–15.20 ± 0.40 Ma (K/Ar ages) (Table 2). Consequently, the radiometric age data from the Dikili–Bergama Region indicate that two distinct sequences were developed. The first was from 18.5 to 16.7 Ma in late Early Miocene and the second was around ~15 Ma in early Middle Miocene (Fig. 4a; Table 2).

The contact relationship between these two volcano-sedimentary units is in question. Akyürek and Soysal (1983), reported that the lower sediments are conformably overlain by the upper sediments. Genç and Yılmaz (2000) pointed out that the contact does not clearly represent any unconformity, but Karacık et al. (2007) pointed out an unconformity.

3.1.3. Foça–Aliağa–İzmir area and surrounding region

In the Foça–Aliağa–İzmir area (lat: 38°.30′; long: 26°.30′–27°.30′; Fig. 2), the Neogene volcano-sedimentary units are represented by a lower and an upper successions. In the Foça–Aliağa–İzmir region, the Early Miocene volcanic rocks of the Yuntdağ volcanics overlie the alluvial-fan and fluvio-lacustrine sedimentary units of the lower sedimentary succession (Dönmez et al., 1998; Altunkaynak et al., 2010; Özkaymak et al., 2013; Uzel et al., 2012; Fig. 4b). The Yuntdağ volcanic complex in the vicinity of Foça–Aliağa area from the Dumanlıdağ caldera is reported to be ~19.2–17.0 Ma (K–Ar ages) (Table 2; Borsi et al., 1972; Ercan et al., 1996). The rhyolitic rocks of the Foça volcanic area are reported to be 16.63 ± 0.84–16.10 ± 0.69 Ma (Ar/Ar ages) (Table 2; Altunkaynak et al., 2010). These ages indicate that the lower sedimentary succession is late Early Miocene in age. The upper sedimentary succession, represented largely by mainly lacustrine limestones and underlying sandstones (Dönmez et al., 1998; Altunkaynak et al., 2010; Özkaymak et al., 2013; Uzel et al., 2012) are intercalated with and conformably overlain by the mafic rocks (Foça alkaline rocks) of 14.73 ± 0.57–14.30 ± 0.30 Ma (Ar/Ar) in Foça (Altunkaynak et al., 2010), indicating that the upper sedimentary unit is Middle Miocene in age.

Between the towns of İzmir and Manisa, the lacustrine sediments of upper sedimentary succession are overlain by sedimentary mafic lava flows (Erkül et al., 2012). There is no radiometric age data from this volcanic unit but it is well correlated with the Akhisar basalt based on their stratigraphy and geochemistry (Ersoy et al., 2010a). The Akhisar basalt yielded 16.72 ± 0.15 Ma Ar/Ar and 16.9 ± 0.3 Ma K–Ar radiometric ages (Table 2) and conformably overlies the conglomerate

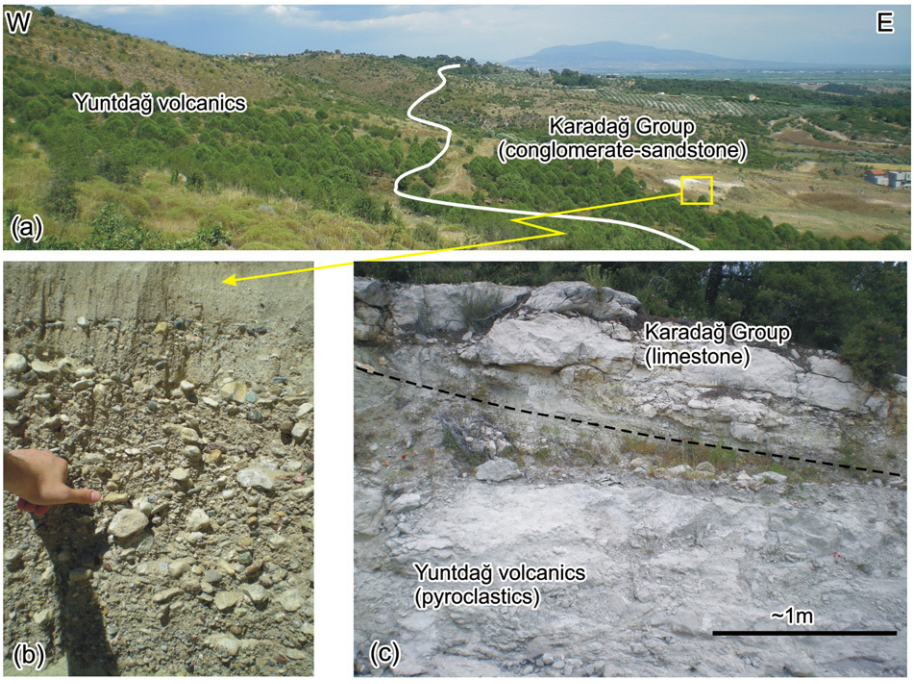

Fig. 5. Field photos showing the stratigraphic relation between the Yuntdağ volcanics and the Karadağ Group along the eastern margin of the Yuntdağ volcanic complex. (a) Yuntdağ volcanics conformably overlying the conglomerates and sandstones of the Karadağ Group in the Üçpınar village, (b) close-up view from the conglomerates and sandstones of the Karadağ Group, showing there is no volcanic clast derived from the Yuntdağ volcanics, (c) limestones of the Karadağ Group conformably overlying the pyroclastic rocks of the Yuntdağ volcanics.

and sandstone units which were previously reported as Late Miocene (Özkaymak et al., 2013) or Middle–Late Miocene (Uzel et al., 2012) in ages. However, the field studies around Üçpınar village (north of Manisa and eastern margin of Yuntdağ volcanic complex), show that the conglomerates and sandstones lie below the andesitic volcanic rocks of the Early Miocene Yuntdağ volcanics and do not contain volcanic clasts (Fig. 5a and b, respectively). Our field observations also indicate that 1) the limestones of the upper sedimentary succession conformably overlie the pyroclastic and epiclastic rocks of the Yuntdağ volcanics (20.42 ± 0.12–17.00 ± 0.30 Ma, Ar/Ar and Rb–Sr ages); and 2) there is no unconformity between the volcanic and sedimentary units (Fig. 5c). These ages clearly suggest that the sandstone–mudstone alternation of the lower sedimentary succession is early Burdigalian in age, and the conglomerates, marls and limestones of the upper sedimentary succession is Langhian in age.

Farther SW, the Neogene stratigraphy of the Karaburun Peninsula (Fig. 2) is characterized by a volcano-sedimentary unit in which several volcanic units have been described. Kaya et al. (2003) stated that, the Early–Middle Miocene fluvio-lacustrine sediments unconformably overlie the felsic pyroclastic rocks, named as Foça tuff (Fig. 4). The andesitic to rhyolitic rocks of 21.3–16.0 Ma (K–Ar and Ar/Ar ages) in the Karaburun Peninsula (Table 2) are interbedded with the sedimentary succession that begins with Bozköy Formation and grades into the Urla limestone (Helvacı et al., 2009). All these volcanic and sedimentary units are overlain by Urla volcanics which were reported as 13.2–11.9 Ma (Borsi et al., 1972; Karacık et al., 2013). Based on K–Ar radiometric age of 11.2 Ma reported by Borsi et al. (1972), the Ovacık basalt in this region has been accepted to be Late Miocene in age. Recently, Karacık et al. (2013) reported 20.00 ± 1.10 Ma K–Ar radiometric age from this unit. Radiometric ages from the volcanic rocks interbedded with sedimentary units in the Karaburun Peninsula are 21.3–16.0 Ma in age, indicating that the sedimentary succession in the area should be considered Early–Middle Miocene in age. The overlying Urla volcanics are Middle Miocene in age.

Southeast of the Karaburun Peninsula, in Cumaovası basin (Uzel and Sözbilir, 2008), the Neogene stratigraphy begins with early Miocene Çatalca Formation, which is unconformably overlain by, in turn, late Miocene–early Pliocene Ürkmez and Yeniköy Formations (Fig. 4d; Genç et al., 2001; Uzel and Sözbilir, 2008). These sedimentary units are conformably overlain by the rhyolitic rocks of the Cumaovası volcanics. Recent K–Ar radiometric ages of Karacık et al. (2013) indicate that the Cumaovası volcanics are late Early Miocene in age (17.90 ± 0.60–17.20 ± 0.50 Ma; Table 2). Overall, the Karaburun Peninsula and Cumaovası basins include a lower and an upper sedimentary unit intercalated with the volcanic rocks. Available data indicate that these units are, in turn, Burdigalian and Langhian in ages.

The Kocaçay Basin (İnci, 1991; Sözbilir et al., 2011) is located between the rocks of the İzmir–Ankara zone and the MEMC (Fig. 2). The basin is the southern extension of the Gördes Basin. The Kocaçay Basin fill starts with conglomerates, coal-bearing fine-grained sediments and limestones of Early–Middle Miocene Vişneli and Dereköy Formations (Fig. 4e). The Vişneli Formation is also interbedded with a tuff unit, which yielded 13.40 ± 0.10 Ma Ar/Ar radiometric age (Sözbilir et al., 2011). These units are unconformably overlain by Middle–Late Miocene mudstones and limestones (Kızılca Formation) and younger sediments (İnci, 1991; Sözbilir et al., 2011).

3.1.4. Söke–Kuşadası–Samos area and surrounding region

In the Söke–Kuşadası area (Fig. 2), the Miocene sedimentary succession begins with conglomerates and overlying sandstone–mudstone alternation and limestones of the Lower Miocene Söke Formation (Gürer et al., 2001; Sümer et al., 2013). This unit is unconformably overlain by the conglomerates (Davutlar conglomerate) and limestones of the Kuşadası Formation (Fig. 4f), which are intercalated, and also overlain, by the Hisartepe volcanics. Ercan et al. (1985) reported 6.99 ± 0.22 Ma K–Ar and Sümer et al. (2013) reported 12.31 ± 0.09 Ma Ar–Ar ages from the Hisartepe volcanics. In the Samos area (Fig. 2), the Miocene stratigraphy begins with late Middle Miocene (Serravallian) and continuous to Early Pliocene (Helvacı et al., 1993; Pe-Piper and Piper, 2007). Several volcanic rocks and dikes in the Samos area have yielded K–Ar radiometric ages between 10.20 ± 0.30 and 7.80 ± 0.50 Ma (Table 2).

3.2. NE–SW-trending Neogene basins on the northern MEMC

The northern MEMC is characterized by several NE–SW-trending Neogene basins where fluvio-lacustrine sediments were deposited together with coeval volcanics and volcanoclastics (Fig. 2). These basins are Uşak–Güre, Selendi, Demirci–Akdere, and Emet basins.

3.3. Uşak–Güre Basin

Previous studies reported that the Uşak–Güre Basin contains two main sedimentary groups separated by a regional unconformity: the Hacıbekir and İnay groups (Fig. 6a; Ercan et al., 1978; Seyitoğlu, 1997a; Çemen et al., 2006; Karaoğlu and Helvacı, 2012). Around Kürtköyü village (north of Uşak), the Hacıbekir Group begins with well-rounded ophiolite-derived conglomerates unconformably overlying the ophiolitic mélange units of the İzmir–Ankara Suture Zone (Fig. 7a). The base of the conglomerates is called the Kürtköyü Formation (Fig. 7b; Ersoy et al., 2010a). The Hacıbekir Group in the Uşak Basin, as well as the ophiolitic rocks of the İASZ, structurally overlies the MEMC along a low angle detachment fault (Karaoğlu and Helvacı, 2012). Field studies also indicate that that the conglomerates of the Kürtköyü Formation in the Uşak Basin do not contain clasts derived from the Menderes Extensional Metamorphic Complex, but contain fragments probably derived from the Lycian Nappes (Ersoy et al, 2005; Fig. 7c). There is no volcanic intercalation in the Hacıbekir Group in the Uşak–Güre Basin, and the age of the group is reported as Early Miocene (Karaoğlu and Helvacı, 2012; Seyitoğlu, 1997a). However, palynological data from the coal-bearing horizons in the Kürtköyü Formation indicate that they are Oligocene in age and represent a brackish-water depositional environment (Ersoy et al., 2005), and the formation is well-correlated with the Oligocene sediments of the Lycian molasse basin in the south (Sözbilir, 2005). Therefore, the base of the basin (i.e. Kürtköyü Formation) should be considered as Oligocene rather than Early Miocene and is probably part of İASZ molasse basins in western Anatolia, Turkey.

The İnay Group, unconformably overlying the Hacıbekir Group is composed of conglomerate, sandstone and mudstone of the Ahmetler formation and marls and limestones of the Ulubey formation. The age of the İnay Group in the Uşak Basin is well-constrained by radiometric age data from the several volcanic intercalations (Fig. 6a; Ercan et al., 1996; Seyitoğlu, 1997a; Karaoğlu et al., 2010). The Elmadağ volcanic center in the northern part of the basin yielded 17.29 ± 0.13–16.28 ± 0.05 Ma Ar/Ar ages (Karaoğlu et al., 2010; Table 3). The andesitic–dacitic rocks of the İtecektepe volcanic center, further south of the Elmadağ, emplaced between 15.04 ± 0.10 and 14.60 ± 0.30 Ma (K–Ar and Ar/Ar ages of Seyitoğlu et al., 1997; Karaoğlu et al., 2010). Farther south, andesitic rocks of the Beydağ volcanic center is dated as 13.10 ± 0.20–12.15 ± 0.15 Ma (K–Ar and Ar/Ar ages of Ercan et al., 1996; Karaoğlu et al., 2010). These ages suggest that the deposition of the İnay Group in the Uşak Basin migrated from north (Late Early Miocene) to south (Late Middle Miocene) with time. Mafic volcanic intercalations in the İnay Group in the Güre Basin were also dated as 16.01 ± 0.08 to 14.20 ± 0.12 Ma (K–Ar and Ar/Ar ages; Table 3). The İnay Group is unconformably overlain by the alluvial-fan conglomerates of the Asartepe Formation in the Uşak–Güre Basin. Mammalian fossil age from the Asartepe formation indicates a late Miocene age (Seyitoğlu et al., 2009). These

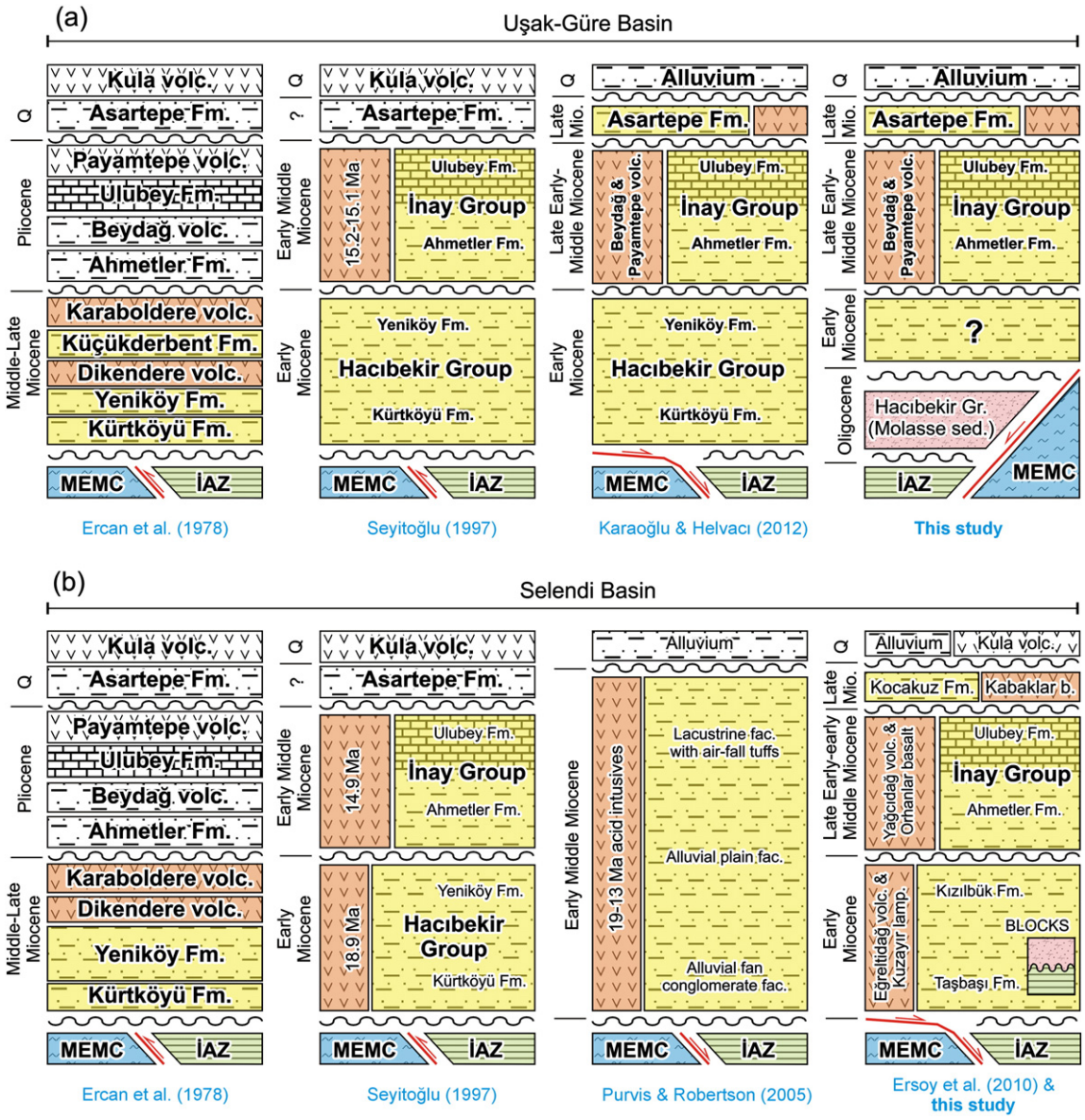

Fig. 6. Comparison of Miocene stratigraphy of the Uşak–Güre (a) and Selendi (b) basins.

sedimentary rocks are cut by the Late Miocene Karaağaç dikes (Karaoğlu et al., 2010).

3.4. Selendi Basin

The Early Miocene sedimentary units in the Selendi Basin, which were dated by using volcanic intercalations, are also known as "*Hacıbekir Group*" (Fig. 6b; Ercan et al., 1978; Seyitoğlu, 1997a; Ersoy et al., 2010a). The Early Miocene sedimentary units in the Selendi Basin begin with conglomerates composed of metamorphic clasts of the MEMC (Fig. 7d; Seyitoğlu, 1997a; Ersoy et al., 2005, 2010a), and also contain olistolites derived from ophiolitic rocks and Jurassic limestones of the İASZ (Ersoy et al., 2010a; Fig. 7e and f). The conglomerates with metamorphic clasts in the Selendi Basin contain some blocks, which are composed of ophiolite-derived well-rounded pebbles (Fig. 7g and h). The lithologies of these blocks are clearly comparable with the ophiolite-derived conglomerates at the base of the Kürtköyü Formation in the Uşak Basin. The olistolits in the Hacıbekir Group are common around the Pabuçlu area to the south of Selendi (Fig. 8). Therefore, we suggest that the Kürtköyü Formation in the Uşak Basin may represent an extensional allochthon. Some blocks from the Hacıbekir Group occur as olistolites in the Early Miocene sedimentary rocks of the Selendi Basin. Therefore, this conglomeratic unit should not be considered as part of the Hacıbekir Group in the Selendi Basin. We suggest that these Early Miocene units could be correlated with those in the Emet Basin, located to the north of the Selendi Basin (see Figs. 6b and 9b for comparison). Consequently, the name "Taşbaşı Formation" for the Early Miocene conglomerates and the name "Kızılbük Formation" for the Early Miocene coal-bearing sandstones may be used in the Selendi Basin. Dacitic–rhyolitic volcanic rocks are also present in the Early Miocene sedimentary rocks of the Selendi Basin (Ersoy et al., 2008). The volcanics (Eğreltidağ volcanics and Kuzayır lamproite) have yielded 20.00 ± 0.20–17.90 ± 0.20 Ma K–Ar and Ar/Ar radiometric ages (Table 3).

The İnay Group in the Selendi Basin is intercalated with the andesitic–dacitic volcanic rocks of the Yağcıdağ volcanics and mafic lavas of the Orhanlar basalt (Fig. 6b; Ersoy et al. 2008, 2010a). The Yağcıdağ volcanics yielded 16.61 ± 0.1–14.90 ± 0.60 Ma Ar/Ar and K–Ar radiometric ages (Seyitoğlu et al., 1997; Purvis et al., 2005; Table 3). The

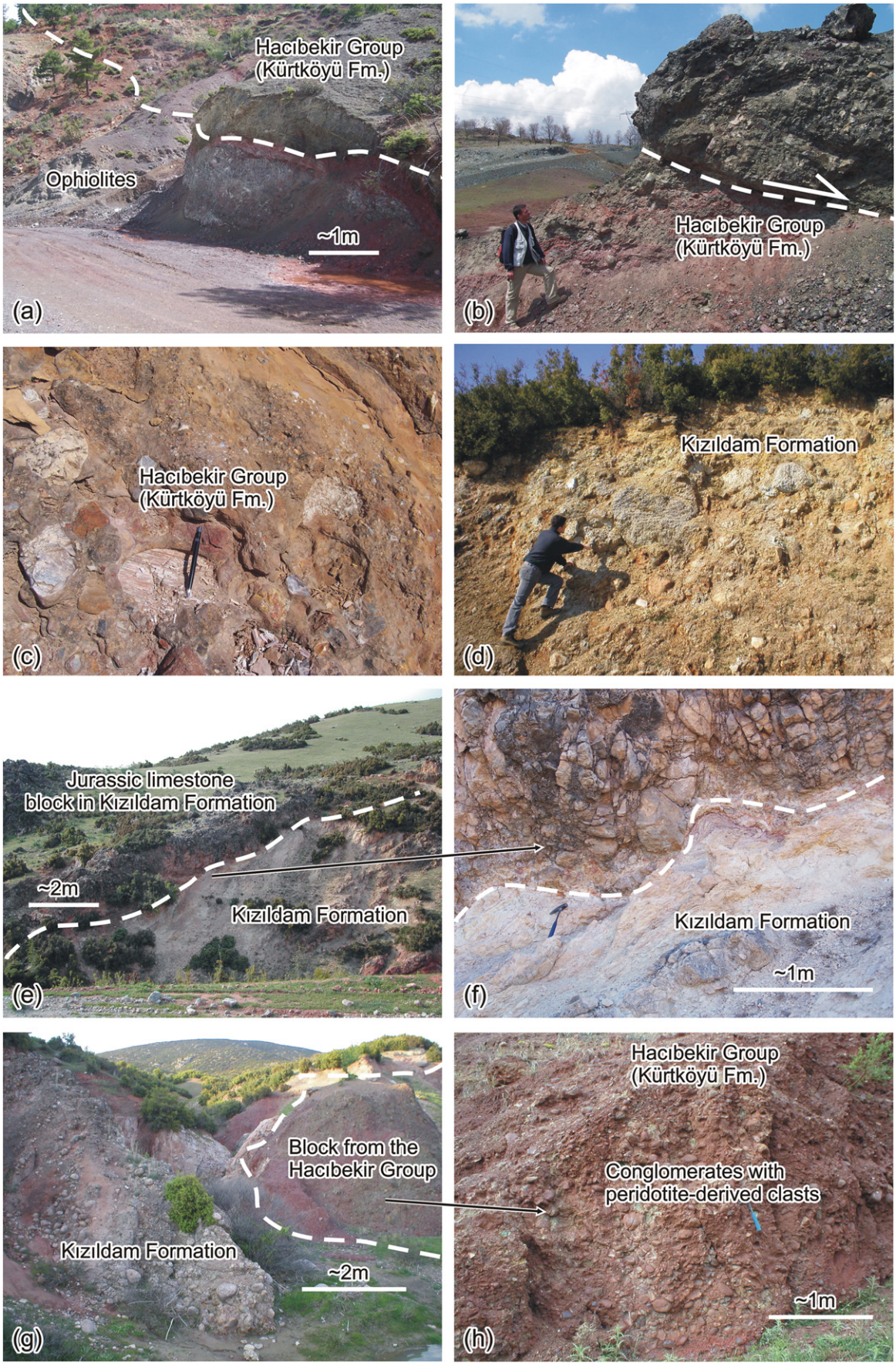

Fig. 7. Field photos from the Kürtköyü Formation of the Hacıbekir Group in Uşak and Selendi basins. See text for explanation. Panel (f) is from Ersoy et al. (2010a).

Table 3
Radiometric age data from the volcanic rocks in the NE–SW-trending basins.

Basin and unit		Sample	Rock type	Radiometric age (Ma), material and reference
Demirci Basin				
Sevinçler volcanics		721	Dacite	19.06 ± 0.05 (plagioclase, Ar/Ar) (Ersoy et al., 2012)
		721	Dacite	19.75 ± 0.07 (biotite, Ar/Ar) (Ersoy et al., 2012)
		721	Dacite	19.75 ± 0.05 (biotite, Ar/Ar) (Ersoy et al., 2012)
		721	Dacite	19.56 ± 0.04 (biotite, Ar/Ar) (Ersoy et al., 2012)
Naşa basalt		ÖD-50	Shoshonite	15.80 ± 0.30 (whole rock, K–Ar) (Ercan et al., 1996)
		ÖD-52	Latite	15.20 ± 0.30 (whole rock, K–Ar) (Ercan et al., 1996)
Asitepe volcanics		717	Andesite	17.58 ± 0.09 (plagioclase, Ar/Ar) (Ersoy et al., 2012)
Taşokçular basalt		727	Shoshonite	10.46 ± 0.03 (whole rock, Ar/Ar) (Ersoy et al., 2012)
Selendi Basin				
Eğreltidağ volcanics		SE-1	Rhyolite	18.90 ± 0.60 (biotite, K–Ar) (Seyitoğlu et al., 1997)
		521	Dacite	18.90 ± 0.10 (plagioclase, Ar/Ar) (Ersoy et al., 2008)
		521	Acidic tuff	20.00 ± 0.20 (amphibole, Ar/Ar) (Ersoy et al., 2008)
Kuzayır lamproite		518	Lamproite	17.90 ± 0.20 (groundmass, Ar/Ar) (Ersoy et al., 2008)
		518	Lamproite	18.60 ± 0.20 (phlogopite, Ar/Ar) (Ersoy et al., 2008)
Yağcıdağ volcanics		SE-3	Trachydacite	14.90 ± 0.60 (biotite, K–Ar) (Seyitoğlu et al., 1997)
		S1/3	Acidic tuff	16.42 ± 0.99 (feldspar, Ar/Ar) (Purvis et al., 2005)
		S1/3	Acidic tuff	16.61 ± 0.14 (biotite, Ar/Ar) (Purvis et al., 2005)
		YF-2	Dacite	16.43 ± 0.32 (plagioclase, Ar/Ar age) (Ersoy et al., 2012)
Orhanlar basalt				Middle Miocene (stratigraphic relations)
Kabaklar basalt		S-1	K-trachybasalt	8.50 ± 0.20 (whole rock, K–Ar) (Ercan et al., 1996)
		IZ-67	K-trachybasalt	8.37 ± 0.07 (whole rock, Ar/Ar) (Innocenti et al., 2005)
Uşak–Güre Basin				
Beydağ volcanics	Elmadağ volc. center	U-31	Trachydacite	16.28 ± 0.05 (biotite, Ar/Ar) (Karaoğlu et al., 2010)
		U-68	Pyroclastic	16.48 ± 0.08 (biotite, Ar/Ar) (Karaoğlu et al., 2010)
		U-70	Latite	16.44 ± 0.07 (groundmass, Ar/Ar) (Karaoğlu et al., 2010)
		U-132	N/A	16.48 ± 0.33 (biotite, Ar/Ar) (Karaoğlu et al., 2010)
		U-164	Trachytic dome	17.29 ± 0.13 (amphibole, Ar/Ar) (Karaoğlu et al., 2010)
	İtecektepe volcanic center	UG-63	Dacite	14.60 ± 0.30 (whole rock, K–Ar) (Seyitoğlu et al., 1997)
		U-159	Dacite dike	15.04 ± 0.10 (biotite, Ar/Ar) (Karaoğlu et al., 2010)
	Beydağ volcanic center	U-2	Dacite	13.10 ± 0.20 (whole rock, K–Ar) (Ercan et al., 1996)
		U-161	Dacitic dome	12.15 ± 0.15 (biotite, Ar/Ar) (Karaoğlu et al., 2010)
Payamtepe volcanics	Yeniköy dikes	UG-58	Trachydacite	15.10 ± 0.40 (whole rock, K–Ar) (Seyitoğlu et al., 1997)
		U-153	Trachyte	16.01 ± 0.08 (sanidine, Ar/Ar) (Karaoğlu et al., 2010)
	Karabacaklar volcanics	UG-75	Trachyte	15.90 ± 0.40 (whole rock, K–Ar) (Seyitoğlu et al., 1997)
		UG-142	Trachyte	15.20 ± 0.60 (whole rock, K–Ar) (Seyitoğlu et al., 1997)
		U-144	Trachyte	15.93 ± 0.08 (groundmass, Ar/Ar) (Karaoğlu et al., 2010)
	Kıran basalt	UG-145	UK Latite	15.50 ± 0.40 (whole rock, K–Ar) (Seyitoğlu et al., 1997)
	Güre lamproite	IZ-38	Lamproite	14.20 ± 0.12 (groundmass, Ar/Ar) (Innocenti et al., 2005)
		05GÜ02	Lamproite	15.54 ± 0.33 (groundmass, Ar/Ar) (Prelević et al., 2012)
		05GÜ02	Lamproite	15.67 ± 0.29 (groundmass, Ar/Ar) (Prelević et al., 2012)
		05GÜ02	Lamproite	15.32 ± 0.25 (groundmass, Ar/Ar) (Prelević et al., 2012)
Emet Basin & Gediz–Şaphane Region				
Akdağ volcanics		E1	Rhyolite	20.30 ± 0.60 (biotite, K/Ar) (Seyitoğlu et al., 1997)
		E6	Rhyolite	20.20 ± 0.40 (biotite, K/Ar) (Seyitoğlu et al., 1997)
		E-3	Rhyolite	19.00 ± 0.20 (biotite, K/Ar) (Helvacı and Alonso, 2000)
Köprücek volcanics		E-1	Pyroclastic	16.80 ± 0.20 (biotite, K/Ar) (Helvacı and Alonso, 2000)
Dereköy basalt		E9	UK latite	15.40 ± 0.20 (feldspar, K/Ar) (Helvacı and Alonso, 2000)
		E3	UK latite	14.90 ± 0.60 (whole rock, K–Ar) (Seyitoğlu et al., 1997)
		So7-15	UK latite	15.70 ± 0.50 (whole rock, K–Ar) (Çoban et al. 2012)
Kestel volcanics		821	UK latite	15.91 ± 0.07 (biotite, Ar/Ar) (Ersoy et al., 2012)
		821	UK latite	15.73 ± 0.11 (biotite, Ar/Ar) (Ersoy et al., 2012)
Ilıcasu lamproite		IZ-41	Lamproite	15.87 ± 0.13 (phlogopite, Ar/Ar) (Innocenti et al., 2005)
		IZ-41	Lamproite	15.83 ± 0.13 (groundmass, Ar/Ar) (Innocenti et al., 2005)
		05IS01	Lamproite	15.54 ± 0.06 (phlogopite, Ar/Ar) (Prelević et al., 2012)
		05IS03	Lamproite	15.77 ± 0.09 (phlogopite, Ar/Ar) (Prelević et al., 2012)
Central Menderes Core Complex				
Toygar andesite (northern shoulder of Gediz Graben)		ÖD-56	Dacite	14.80 ± 0.40 (whole rock, K–Ar) (Ercan et al., 1996)
		S1/30	Andesite	16.08 ± 0.91 (feldspar, Ar/Ar) (Purvis et al., 2005)
		S1/30	Andesite	14.65 ± 0.06 (biotite, Ar/Ar) (Purvis et al., 2005)
Başova andesite (Küçük Menderes Graben)		BR-01	Dacite	14.70 ± 0.10 (whole rock, Ar–Ar) (Emre and Sözbilir, 2005)
		YN-01	Dacite	14.30 ± 0.10 (whole rock, Ar–Ar) (Emre and Sözbilir, 2005)
		ÖD-14	Andesite	15.60 ± 0.30 (whole rock, K–Ar) (Ercan et al., 1996)
		ÖD-16a	Andesite	13.80 ± 2.00 (whole rock, K–Ar) (Ercan et al., 1996)
		ÖD-16b	Andesite	17.90 ± 2.40 (whole rock, K–Ar) (Ercan et al., 1996)

İnay Group is unconformably overlain by the alluvial-fan conglomerates, Kocakuz Formation, in the Selendi Basin. The Kocakuz Formation is overlain by the Kabaklar basalt which yielded 8.50 ± 0.20 Ma Ar/Ar radiometric age (Ercan et al., 1996; Innocenti et al., 2005; Table 3).

3.5. Demirci–Akdere and Emet basins

The Demirci Basin is located between the Gördes and Selendi basins, and developed between NE and SW-trending structural highs where metamorphic rocks of MEMC are exposed at the surface (Fig. 2). The

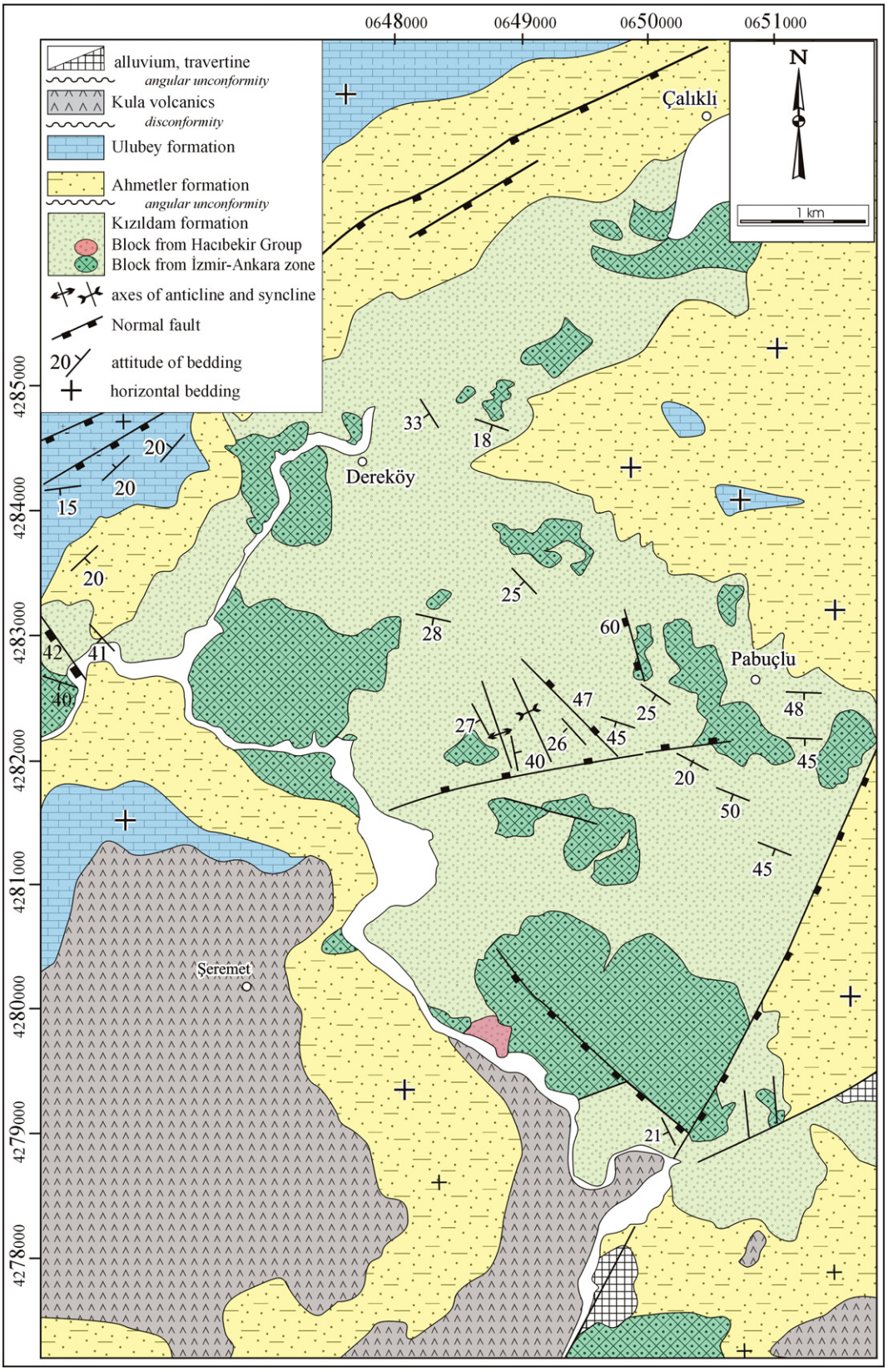

Fig. 8. Geological map of the Dereköy area to the SW of Selendi in Selendi Basin.

Demirci–Akdere Basin was cut by the Pliocene–Quaternary Simav graben. The northern part is known as Akdere Basin; while the southern part is know as Demirci Basin. Neogene units of these basins were studied in detail by İnci (1984), Seyitoğlu (1997b), Yılmaz et al. (2000) and Ersoy et al. (2011) (Fig. 9a). The Neogene sedimentary succession in the Demirci Basin begins with Early Miocene sedimentary and volcanic rocks, observed mainly in the northern part of the basin. These units have previously been correlated with the Hacıbekir Group

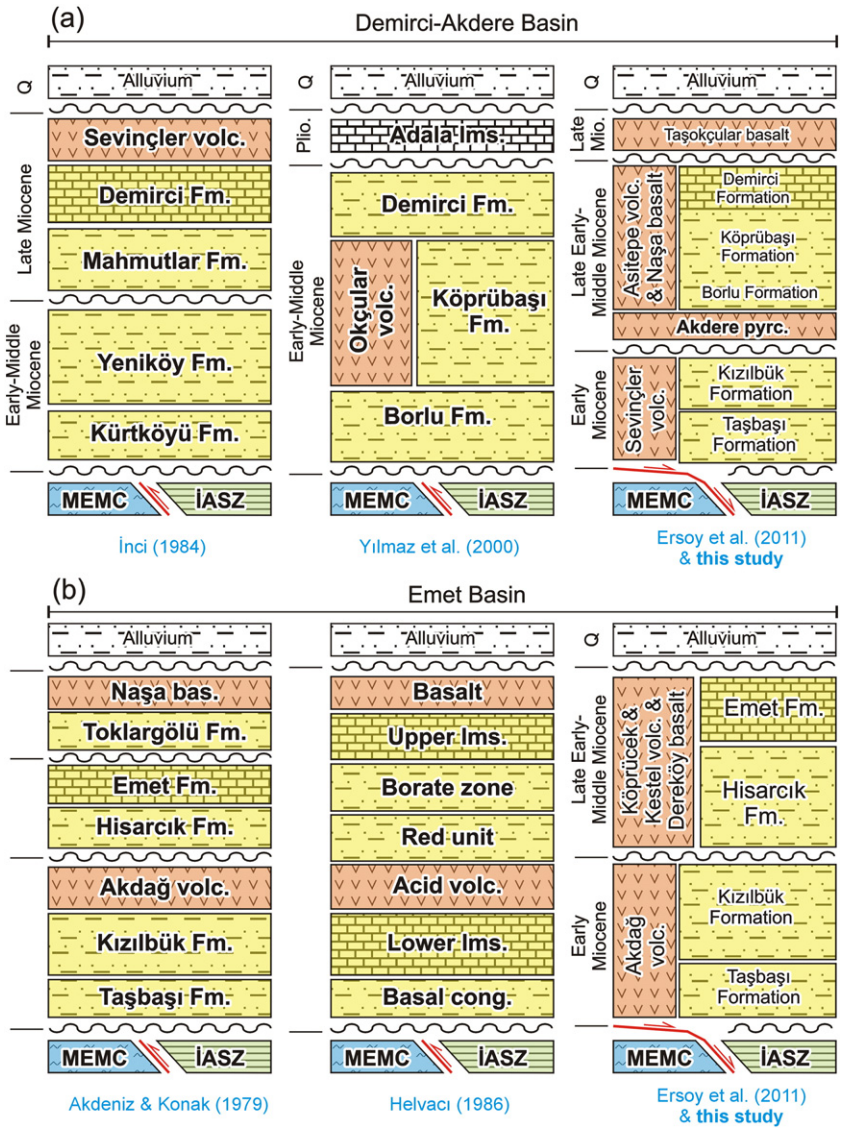

Fig. 9. Comparison of Miocene stratigraphy of the Demirci–Akdere (a) and Emet (b) basins.

of the Uşak–Güre Basin (Ersoy et al., 2011, İnci, 1984). However, lithological and age data presented here indicate that they should be correlated with the Taşbaşı (conglomerates composed of metamorphic and granitic clasts) and Kızılbük (yellowish sandstones) formations of the Emet and Selendi basins. The Taşbaşı and Kızılbük formations are conformably overlain by the dacitic–rhyolitic volcanic rocks of the Sevinçler volcanics, which are correlated with the Eğreltidağ volcanics in the Selendi Basin. Ersoy et al. (2012) reported 19.75 ± 0.05 to 19.06 ± 0.05 Ma Ar–Ar ages from the Sevinçler volcanics (Table 3) indicating an Early Miocene (Burdigalian) age.

The Taşbaşı and Kızılbük formations are unconformably overlain by a volcano-sedimentary unit, which is composed, from bottom to top, of felsic tuffs of Akdere pyroclastics, boulder conglomerates of Borlu Formation, mudstone–sandstone alternation of the Köprübaşı Formation and marls and limestones of the Demirci Formation. The Köprübaşı Formation is intercalated with andesitic–dacitic rocks of the Asitepe volcanics and mafic lava flows of the Naşa basalt. Plagioclase separates from an andesite sample of Asitepe volcanics yielded 17.58 ± 0.09 Ma (Ersoy et al., 2012), indicating that the transition from Köprübaşı to Demirci formations occurred during late Early Miocene (Burdigalian). The Naşa basalt yielded 15.80 ± 0.30–15.20 ± 0.30 Ma K–Ar radiometric ages (Ercan et al., 1996), indicating that the deposition of the Köprübaşı Formation continued up to early Middle Miocene (latest Burdigalian–early Langhian). In the Demirci Basin, a small basaltic occurrence in the southern part of the Asitepe volcanic center, the Taşokçular basalt, is dated as 10.46 ± 0.03 Ma (Ar/Ar age, Table 3, Ersoy et al., 2012), indicating the presence of Late Miocene basaltic activity in the basin.

The Emet Basin is located to the north of the Selendi and Uşak–Güre basins (Figs. 2 and 9b). The basin fill starts with conglomerates of Taşbaşı Formation with clasts mainly derived from augen gneisses and schists of the MEMC. The section grades upward s into yellowish sandstones of Kızılbük Formation (Akdeniz and Konak, 1979; Ersoy et al., 2011; Helvacı, 1986; Helvacı and Alonso, 2000). These units are interfingered with dacitic–rhyolitic volcanic rocks of the Akdağ volcanics, which are geochemically and stratigraphically well-correlated with the Sevinçler volcanics in the Demirci Basin and Eğreltidağ volcanics in the Selendi Basin (Ersoy et al., 2012). The Akdağ volcanics yielded 20.30 ± 0.60 to 19.00 ± 0.20 Ma K–Ar ages (Table 3; Seyitoğlu et al., 1997; Helvacı and Alonso, 2000), indicating that the Taşbaşı and Kızılbük formations were deposited during Burdigalian. This volcano-sedimentary unit in the Emet Basin is unconformably overlain, in turn, by the borate bearing sandstone–claystone alternation of the Hisarcık formation and the limestones of the Emet formation, which are interfingered with the Köprücek volcanics in the northern part of the basin and by the Dereköy basalt in the

southern part of the basin. Helvacı and Alonso (2000) have reported 16.80 ± 0.20 Ma Ar/Ar age from the Köprücek volcanics. The Dereköy basalt yielded 15.70 ± 0.50 to 14.90 ± 0.60 Ma K–Ar ages (Table 3; Seyitoğlu et al., 1997; Helvacı and Alonso, 2000; Çoban et al., 2012). Ersoy et al. (2012) have also presented 15.9–15.7 Ma ages from the Kestel volcanics cutting the Kızılbük Formation. These ages indicate that the borate-bearing sedimentary units were deposited between late Burdigalian and early Langhian.

3.6. Volcanic units in central Menderes Extensional Metamorphic Core Complex

There are small-volume volcanic units emplaced in the northern edge of the Gediz (Alaşehir) Graben (the Toygar andesites) and northern margin of the Küçük Menderes Graben (The Başova andesites) (Fig. 2). The Toygar andesites yielded 14.80 ± 0.40 Ma K–Ar (Ercan et al., 1996) and 16.08 ± 0.91–14.65 ± 0.06 Ma Ar/Ar ages (Purvis et al., 2005). The Başova andesite in the Küçük Menderes Graben yielded 17.90 ± 2.40 to 13.80 ± 2.00 Ma K–Ar ages (Ercan et al., 1996). More reliable Ar/Ar age determinations from this volcanic unit yielded 14.70 ± 0.10 and 14.30 ± 0.10 Ma (Emre and Sözbilir, 2005).

4. New age data

During this investigation, we have obtained $^{40}Ar/^{39}Ar$ radiometric age data from six strategic samples from areas where critical stratigraphic and structural relationships were in question (Fig. 9). One of the areas is the Soma Basin where we collected samples 915 and 115 from Dededağ and Asartepe localities. These samples are gray- to black-colored andesitic lava flows which conformably overlie the Deniş Formation of İnci (1998) (Fig. 10). Previous studies described this volcanic units as "basaltic extrusions" of late Miocene, However, no radiometric ages have been reported. Therefore the radiometric age of these units are important to provide exact ages of these volcanic rocks. The samples 128 and 116 are from north of Göçbeyli and SW of Soma (Fig. 10), where pink colored andesitic lava flows conformably overlie the Deniş Formation of İnci (1998). Samples 124 and 911 are from a basaltic dike in Adilköy volcanics rocks which, cut the coal-bearing sediments of the Soma Formation and is called the Saricakaya dike.

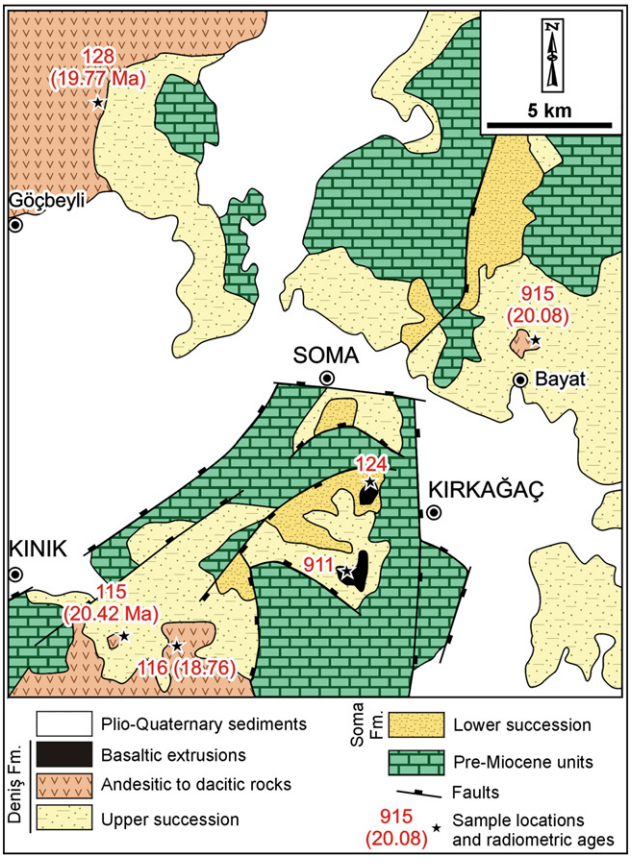

Fig. 10. Geological map of the Soma Basin showing the locations of the volcanic rocks with radiometric age determination.
Map is from İnci (2002).

4.1. Analytical methods for Ar/Ar geochronology

$^{40}Ar/^{39}Ar$ geochronology was carried out on whole rock and biotite samples at The Auburn University Noble Isotope Mass Analysis Laboratory (ANIMAL). The rock samples were selected after petrographic analysis of thin sections from each sample. The selected samples were crushed and sieved for whole rock and biotite grains. The individual whole rock (250–212 μm) and biotite (850–600 μm) grains were hand-picked under a binocular microscope to be generally free from visible inclusion of other phases and free from visible alterations. The selected samples were washed with de-ionized water in ultrasonic cleaner.

Samples were located in aluminum disk with monitor FC-2 (age = 28.02 Ma, Renne et al., 1998) along with CaF_2 flux monitor. All samples and standards were irradiated in the USGS TRIGA reactor located at the Denver Federal Center, USA. The ANIMAL analytical lab is equipped with a low-volume, high sensitivity 10 cm radius sector mass spectrometer and automated sample extraction system (50 W Syndrad CO_2 laser). The analyses of these samples were conducted by laser incremental heating analysis (LIH) of approximately 100 grains of whole rock. The biotite samples were dated from single crystal total fusion (SCTF) and single crystal incremental heating method (SCIH).

All statistical $^{40}Ar/^{39}Ar$ ages in this study (weighted means, plateau, or isochron) are quoted at the standard deviation in precision of measurement, whereas errors in individual measurements are quoted at one standard deviation. Data reduction was calculated through use of custom Microsoft Excel application. The plateau and correlation ages were calculated by isoplot (Ludwig, 2003). Plateau in this study was defined as at least three or more contiguous increments containing more than 50% of the ^{39}ArK in three or more contiguous steps with no resolvable slope among ages.

4.2. Results and comparison of Ar/Ar geochronology

The whole rock and single grain plateau ages were obtained by laser controlled incremental heating (for minerals 15–18 and whole rock 20–29 increments) to provide more detail on the outgassing behaviors of the samples. SCTF ages were achieved from biotite samples. The results are given in Appendix 1 and Fig. 11.

SCIH biotite ages, samples 128 and 116, yielded well-developed plateau ages of 19.77 ± 0.03 (MSWD = 0.97) and 18.76 ± 0.05 Ma (MSWD = 0.80), respectively, including 100% of the released ^{39}Ar (Fig. 11a and c). SCTF analysis of 19 biotite grains from sample 128 resulted in an age range from 20.50 ± 0.19 to 19.77 ± 0.06 Ma (Fig. 11b). The two biotite grains which yielded older age were rejected by the isoplot program due to extraneous argon. The cumulative probability plot has nearly single mode distribution. The weighted mean age of a total of 17 samples was calculated as 19.91 ± 0.05 Ma (MSWD = 1.9). The 17 biotite grains which were fused from sample 116, gave an age range from 18.90 ± 0.09 to 18.63 ± 0.08 Ma (Fig. 11d). The cumulative probability plot has single mode distribution, which is typical for homogeneous data. The weighted mean age of a total of 17 samples was calculated as 18.77 ± 0.03 Ma (MSWD = 1.08). The SCIH and SCTF ages that resulted from the samples 128 and 116 are compatible. SCIH age is taken as the best estimate for both samples. The age data indicate

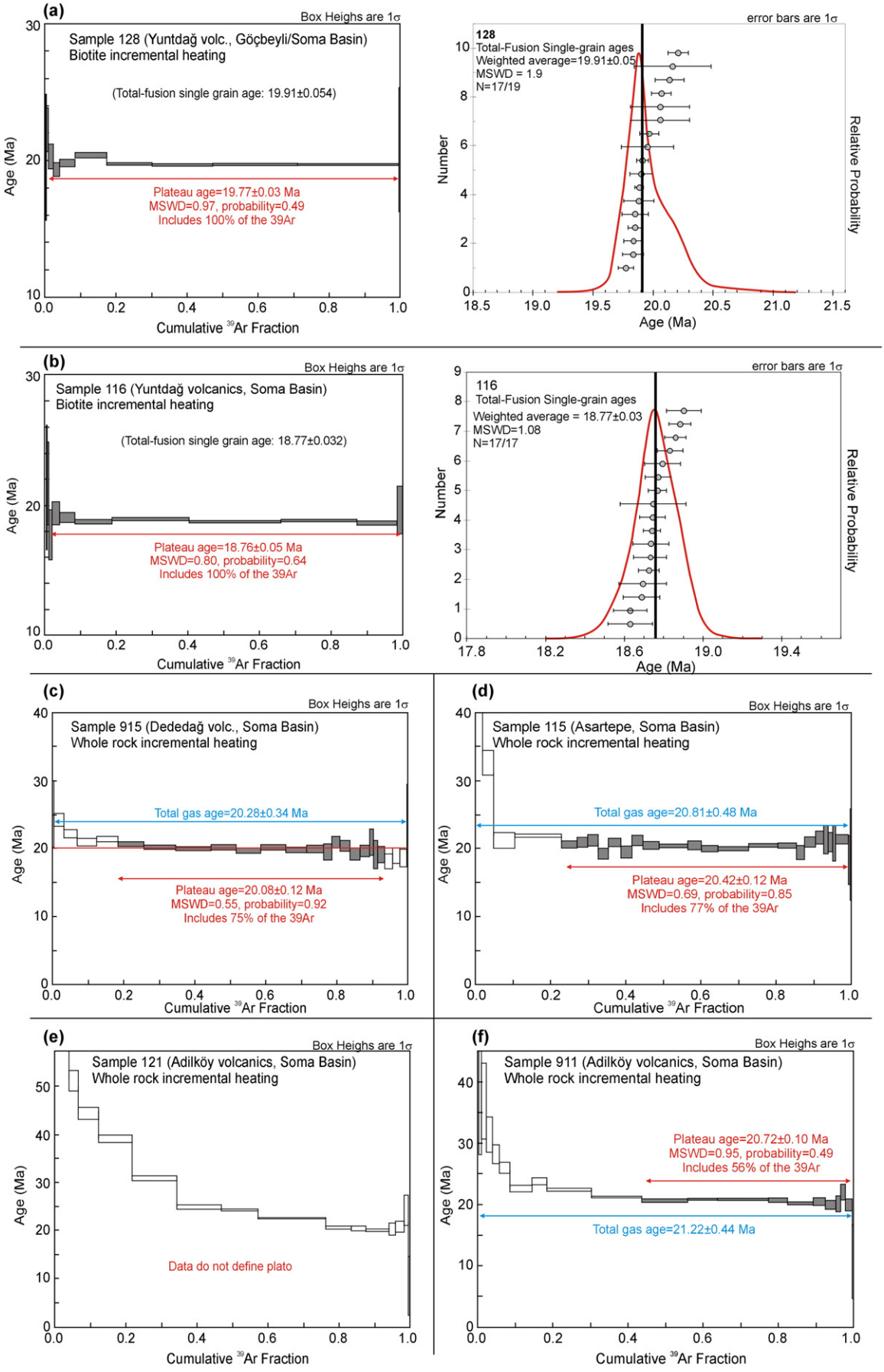

Fig. 11. Results of $^{40}Ar/^{39}Ar$ geochronology of the volcanic rocks from the Soma Basin and adjacent areas.

that the pink-colored andesitic rocks conformably overlying the Deniş Formation is also Burdigalian in age, revealing again that the Deniş Formation should be slightly earlier than Burdigalian. Nearly 1 Ma hiatus between these samples may be related to multi-phase emplacement of the andesitic volcanic complexes. The whole rock samples, 915 and 115 from the Dededağ and Asartepe volcanics in the Soma Basin yielded plateau ages of 20.08 ± 0.12 (MSWD = 0.55), 20.42 ± 0.12 Ma (MSWD = 0.69), with 75% and 77% released ^{39}Ar, respectively (Fig. 11e and f). Total gas ages of these samples are, in turn, 20.28 ± 0.34 and 20.81 ± 0.48 Ma.

The samples 121 and 911 (Sarıcakaya dike of Adilköy basalt) both showed a descending staircase pattern, indicating the presence of excess argon (Fig. 11g and h). The sample 121 did not define plateau but sample 911 yielded a plateau age of 20.72 ± 0.1 Ma (MSWD = 0.95, 56% released ^{39}Ar). Although the sample 911 yielded a plateau, this result is inaccurate because the laser step-heating averaged the heterogeneous components and forced the sample to yield a plateau. Both samples display argon loss and excess argon because of the alteration in the sample, and hence these ages should be tested by further studies.

5. Summary and conclusions

Exhumation of the MEMC was developed in two extensional stages in Early and Middle Miocene (e.g., Ersoy et al., 2011; Lips et al., 2001; Ring et al., 2003). The first stage was asymmetrical and occurred along the north-dipping Simav Detachment Fault (Çemen et al., 2006; Işık and Tekeli, 2001; Işık et al., 2000). During the second stage, the central part of the Menderes massif symmetrically exhumed along the north-dipping Gediz (Alaşehir) and south-dipping Büyük Menderes detachment faults (Fig. 2). There may also be an earlier stage of extension in Late Oligocene as suggested by Lips et al. (2001), Çemen et al. (2006), van Hinsbergen (2010) and Jolivet et al. (2013).

The Neogene basins developed on the MEMC contain two main volcano-sedimentary successions: a lower and an upper volcano-sedimentary unit (İnay Group). Radiometric age determinations together with palynologic data strongly suggest that the lower volcano-sedimentary unit in the Uşak–Güre Basin (originally named as Hacıbekir Group) differs from those in the Demirci–Akdere, Selendi and Emet basins. The conglomerates of the Hacıbekir Group in the Uşak Basin do not contain metamorphic clasts from the MEMC; rather they contain conglomerates derived from the Lycian Nappes, This observation suggest that the lower volcano-sedimentary unit in the Uşak–Güre Basin was deposited before the exhumation of the MEMC. There is no volcanic intercalation in these sediments, and pollen associations from the coal-horizons indicate an Oligocene age. Basal parts of the conglomerates also include shear zones indicating an NE-directed transportation. Therefore, these sediments should be correlated with the Lycian Molasse basin (Sözbilir, 2005) to the south, and were probably tectonic during the first-stage exhumation of the MEMC (Fig. 2).

The peridotitic conglomerates of the Hacıbekir Group in the Uşak–Güre Basin and the Jurassic limestones and ophiolitic mélange rocks of İzmir–Ankara Suture Zone (IASZ) are also found as olistolites in the Early Miocene sediments in the Selendi Basin. These conglomerates contain metamorphic clasts derived from MEMC, and are overlain by turbiditic sandstones which are intercalated with 20–19 Ma dacitic–rhyolitic volcanic rocks (Ersoy et al., 2010a). All these units tectonically overly the MEMC high-grade metamorphic rocks along the Early Miocene Simav Detachment Fault (Ersoy et al., 2010a; Işık and Tekeli, 2001). These observations suggest that the Early Miocene sediments in the Selendi Basin (and Demirci–Akdere and Emet basins) were deposited in supra-detachment basins during exhumation of the MEMC along the Simav Detachment Fault in Early Miocene. During this stage, blocks of Jurassic limestones and ophiolitic mélange units of the İzmir–Ankara Suture Zone, as well as Lycian Molasse basin, were emplaced as olistolites into the supra-detachment basins. As a result, conglomerates of the Hacıbekir Group in the Uşak–Güre Basin represent remnants (as extensional allochthonous) of the Lycian Molasse Basin, which were transported from south to north, during the first-stage exhumation of the MEMC which gave way to the formation of the supra-detachment basins in the upper plate.

The Early Miocene sediments in the NE–SW-trending basins are unconformably overlain by the upper volcano-sedimentary unit (the İnay Group), which contains volcanic intercalations emplaced between ~17.5 and 15 Ma (Burdigalian–Langhian) in Demirci–Akdere, Selendi and Emet basins, and between 17.3 and 12.2 Ma (Burdigalian–Serravallian) in the Uşak–Güre Basin. This suggests that, Miocene volcanism migrated from north to south only in the Uşak–Güre Basin. However, a southerly migration can be ruled out for the Emet and Selendi basins because mafic volcanism at 15 Ma occurred in the two basins (Figs. 6b and 9b). Similarly, there are also volcanic rocks in the east-central part of the MEMC of ~15 Ma (see Fig. 2 and Table 3). Deposition of the İnay Group in the NE–SW-trending MEMC basins was controlled by NE–SW-trending oblique-slip faults (e.g., Ersoy et al., 2010a; Çemen et al., 2012). These faults and the basins do not continue to the south and do not cut the central part of the MEMC, to the south of the Gediz (Alaşehir) Graben. Therefore, they seem to be developed on the hanging-wall of the Gediz (Alasehir) detachment fault that formed during the exhumation of the MEMC. Therefore, we propose that the deposition of the İnay Group on the MEMC was controlled by the NE–SW-trending oblique accommodation faults, as suggested by Şengör et al. (1985) and Çemen et al. (2006).

The Early to Middle Miocene units in the NE–SW-trending basins developed on the MEMC were also cut and deformed by NE–SW-trending right-lateral and NW–SE-trending left-lateral high-angle strike-slip faults, defining a pure shear deformation (Ersoy et al., 2010a, 2011). Clastic rocks were deposited in association with basaltic volcanism extruded along these fault zones and associated small basins (Ersoy et al., 2010a; Karaoğlu and Helvacı, 2012; Seyitoğlu et al., 2009). Radiometric age determination from the basaltic rocks and mammalian fossils in the clastic sedimentary units suggest that these faults and associated basins were formed during ~10.5 to 8 Ma interval (Tortonian). After this period of deformation and associated sedimentation and volcanism, a new period of extensional deformation was initiated and ~E–W-trending high-angle normal faults formed the present day E–W grabens (e.g., Simav, Gediz, and Küçük Menderes Grabens) that cut and displace the earlier NE–SW-trending basins. Although, some NE–SW-trending faults also exist to the south of the Gediz (Alaşehir) graben cutting the E–W-trending normal faults (Çiftçi and Bozkurt, 2009, 2010; Koçyiğit et al., 1999; Öner and Dilek, 2013), these faults should be younger than NE–SW-trending faults bordering the NE–SW-trending basins in the north. The last extensional stage is probably related to the formation of the North and East Anatolian faults around 5 Ma and associated with the westward escape of the Anatolian plate (Çemen et al., 1999, 2006; Şengör and Yılmaz, 1981; Şengör et al, 1985).

While, the Neogene basins developed on the MEMC show rather uniform Miocene stratigraphy (Fig. 12b), radiometric age determinations of the volcanic rocks together with stratigraphic relationship of the Neogene volcano-sedimentary units in the western part of the MEMC suggest that sedimentation migrated from N–NW to S–SW with time. These basins roughly coincide with the wide zone that is defined as the İzmir–Balıkesir Transfer Zone (İBTZ). Fig. 12a shows the exact ages and stratigraphic relationships of the Miocene sedimentary successions in these basins. Sedimentation and volcanism throughout this region were controlled mainly by NE–SW striking , and subsidiary NW–SE striking strike-slip faults and associated basins (e.g., Erkül et al., 2005; Ersoy et al., 2011; Kaya et al., 2007; Sözbilir et al., 2011; Uzel et al., 2013). Early Miocene NW–SE-striking strike-slip faults are described in the Bigadiç (Erkül et al., 2005) and Gördes basins (Ersoy et al., 2011). The eastern margin of the Gördes Basin (Fig. 2) contains NE–SW-striking strike-slip faults, controlling

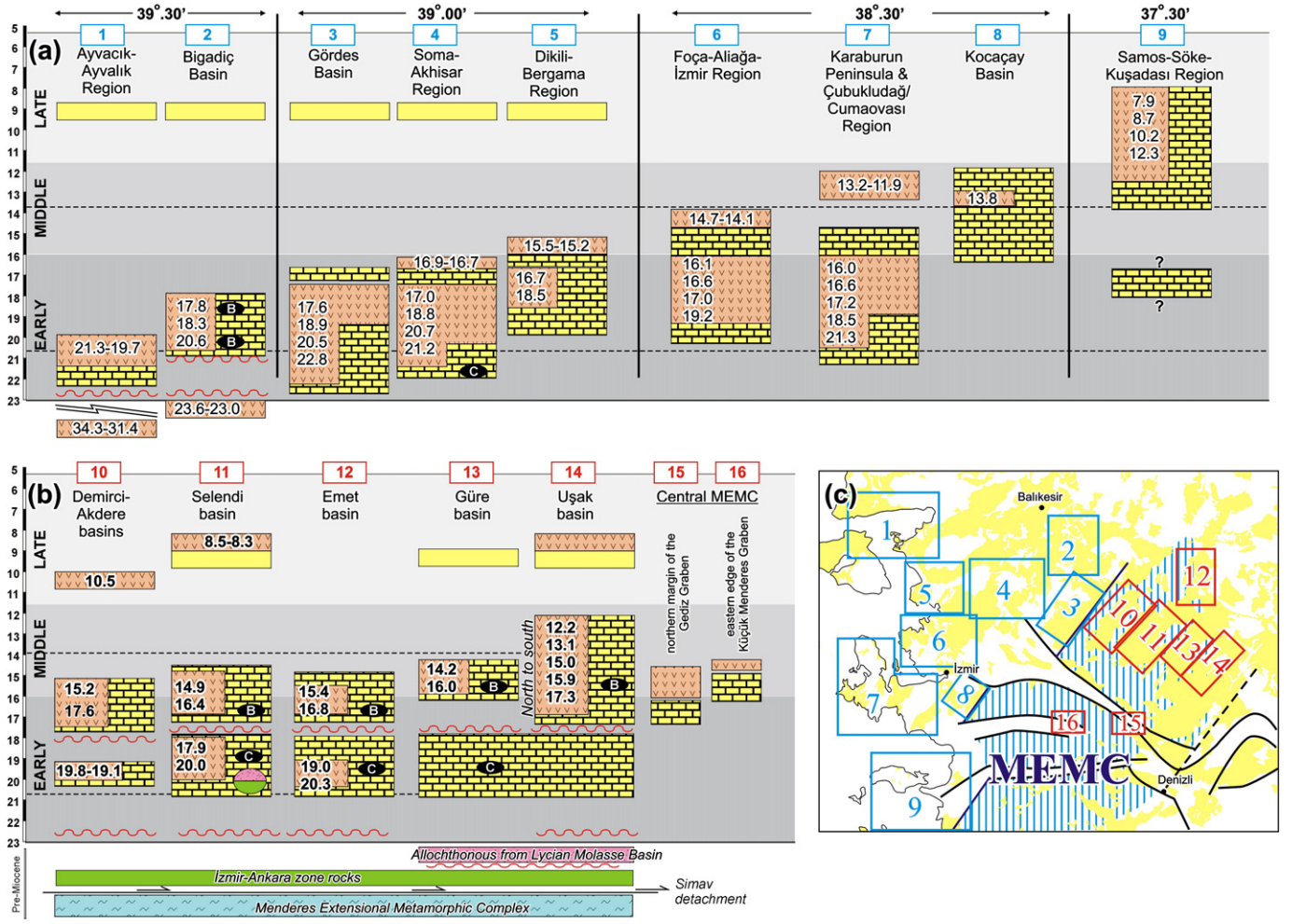

Fig. 12. Miocene stratigraphy of the Neogene basins along the western part of the Menderes Extensional Metamorphic Complex (MEMC) (a) and on the MEMC (b). B and C in the columns indicate borate and coal deposits, respectively. The locations of the columnar sections are given in (c), which also show the distributions of the metamorphic rocks of the MEMC (blue) and the Miocene volcanic/sedimentary units (yellow). See text for details. LSU and USU are Lower and Upper Sedimentary Units, respectively. Note that the ages of the volcano-sedimentary units clearly decrease from N (and NE) to S (and SW).

the Early Miocene sedimentation (Ersoy et al., 2011). This indicates that exhumation along the western side of the MEMC was controlled by the strike-slip faults which were accommodating the Early Miocene NE-dipping low-angle detachment fault (i.e., Simav Detachment Fault). In the Dikili–Bergama area, Early–Middle Miocene sedimentation was controlled by NE–SW- and NW–SE-striking strike-slip faults (Genç and Yılmaz, 2000; Karacık et al., 2007). In the Foça area, Middle Miocene mafic lavas and dikes were emplaced along the N–S to NE–SW-striking strike-slip faults (Altunkaynak et al., 2010). In the Karaburun peninsula, Early–Middle Miocene volcanic rocks were emplaced along N–S-striking strike-slip faults (Helvacı et al., 2009). Middle Miocene sedimentation in the Kocaçay Basin is interpreted as controlled by NE–SW-striking strike-slip faults (Sözbilir et al., 2011). Emplacement of the Tortonian dikes in the Samos island was also controlled by N–S to NE–SW-striking faults (Pe-Piper et al., 2002). The data summarized above suggest that sedimentation and volcanism in the western part of the MEMC migrated, in general, from north to south via a set of NE–SW-trending strike-slip deformation zone (Figs. 2 and 12) (Boccaletti et al., 1974; Erkül et al., 2005; Kaya, 1981; Kaya et al., 2007; Uzel and Sözbilir, 2008; Uzel et al., 2013; Walcott and White, 1998). This deformation zone is frequently described in the literature as the İzmir–Balıkesir Transfer Zone (İBTZ) whose southern continuation is known as the mid-Cycladic lineament in south Aegean Sea (Boccaletti et al., 1974; Erkül et al., 2005; Ersoy et al 2010b; Uzel and Sözbilir, 2008; Uzel et al., 2013).

The available published palaeomagnetic data indicate that (1) the Aegean crust in Greece rotated clockwise while the crust in western Turkey rotated anticlockwise, and (2) complex deformation occurred around Karaburun Peninsula and Chios Island (e.g., Kissel and Laj, 1988; Kissel et al., 1987; 2003; Kondopoulou et al., 2011; van Hinsbergen et al., 2005). The data also suggest that the clockwise rotation to the west of the İBTZ, has occurred around a pole in northern Greece, which was resulted from rotational retreatment (i.e., slab-rollback) of the Hellenic subduction zone because the eastern edge of the subduction zone retreated faster than its western part (Brun and Sokoutis, 2012; Kissel et al., 2003; van Hinsbergen and Schmid, 2012).

Rotational rollback of the Aegean slab along the Hellenic subduction zone crated a rotational extension and associated strike-slip deformation zone in the overriding plate as demonstrated by the analog models of Schellart et al. (2003). Ersoy and Palmer (2013) suggested that the outermost part of this rotational extension area is represented by the NE–SW-trending strike-slip faulting, which corresponds roughly to the İBTZ. Along the outermost part of the rotational area, deformation, sedimentation and volcanism migrate from N–NE to S–SW, as suggested by the deformational history and stratigraphy of the Miocene rock units along the western margin of the MEMC (Fig. 12a). Therefore, we suggest that the southward younging of Neogene sediments and volcanics is related to rotational extension in the Aegean Extensional Province (Fig. 13). In this case, strike-slip deformation in this region (known as İzmir–Balıkesir Transfer Zone) should simply be

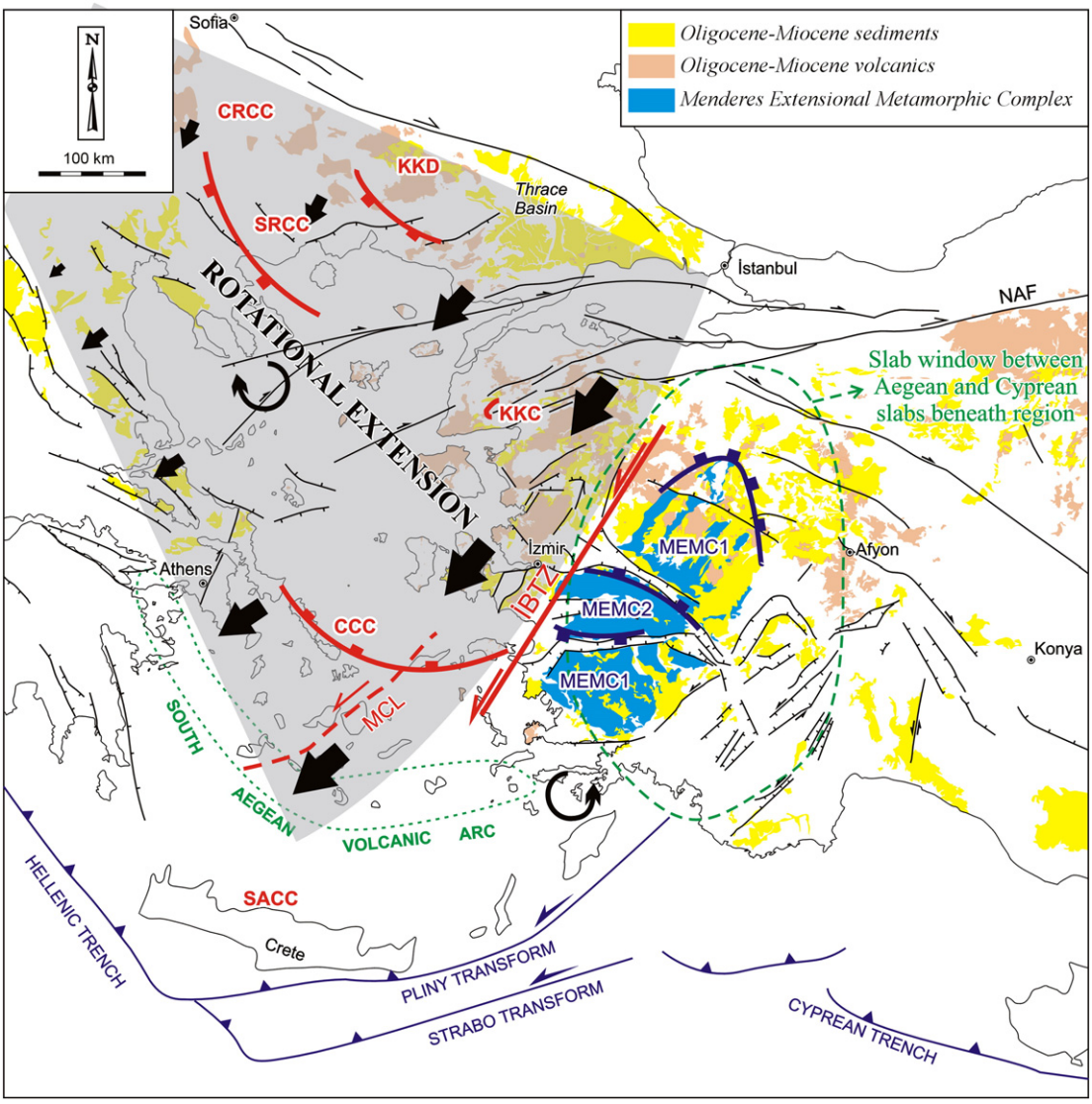

Fig. 13. Geological map showing the distribution of the Menderes Extensional Metamorphic Complex (MEMC), Oligocene–Miocene volcanic and sedimentary units and volcanic centers in the Aegean Extensional Province (compiled from geological maps of Greece (IGME) and Turkey (MTA), and adapted from Ersoy and Palmer, 2013). Extensional deformation field with rotation (rotational extension) is shown with gray field, and simplified from Brun and Sokoutis (2012), Kissel et al. (2003) and van Hinsbergen and Schmid (2012). İzmir–Balıkesir Transfer zone (İBTZ) give the outer limit for the rotational extension, and also limit of ellipsoidal structure of the MEMC. MEMC developed in two stages: the first one was accommodated during early Miocene by the Simav Detachment Fault (SDF) in the north; and the second one developed during Middle Miocene along the Gediz (Alaşehir) Detachment Fault (GDF) and Küçük Menderes Detachment Fault (KMDF). Extensional detachments were also accommodated by strike-slip movement along the İBTZ (Ersoy et al., 2011) and Uşak–Muğla Transfer Zone (Çemen et al., 2006; Karaoğlu and Helvacı, 2012). Other main core complexes in the Aegean, the Central Rhodope (CRCC), Southern Rhodope (SRCC), Kesebir–Kardamos Dome (KKD) and Cycladic (CCC) Core Complexes are also shown. The area bordered with dashed green line represents the surface trace of the asthenospheric window between the Aegean and Cyprean subducted slabs (Biryol et al., 2011; de Boorder et al., 1998). See text for detail.

related to the eastern (outermost) border of this rotational extension. The rate of extension also increases from the pole to the outer zone. This is evidenced by basin formation and extensive volcanic activity along the wide İBTZ. Moreover, van Hinsbergen and Schmid (2012) suggested that the rotational extension did not occur around a single pole, rather it evolved by a set of poles, around which rotational extension occurred. They stated that the poles have migrated from north to south. For simplicity, a single rotational extensional area has been constructed in Fig. 13.

Effects of the rotational extension in the Aegean Region wane along the İBTZ towards east. The İBTZ also forms the western margin of the MEMC (Fig. 13). This also suggests circuitously that the subducted Aegean slab is rotationally rolling back. Mantle tomography studies in the region show the presence of a low-velocity zone, related to an asthenospheric upwelling along a window below the MEMC (Biryol et al., 2011; de Boorder et al., 1998; van Hinsbergen et al., 2010b). The MEMC may have developed in response to asthenospheric upwelling and associated isostatic rebound from this window between the subducted Aegean (to the west) and Cyprean (to the east) slabs (Ersoy and Palmer, 2013; Gessner et al., 2013; Prelević et al., 2012).

Acknowledgment

The preliminary conclusions of this study were presented during International Earth Science Colloquium on the Aegean Region, IESCA, which was held in Dokuz Eylül University, İzmir, Turkey (1–5 October 2012). We thank three anonymous reviewers for their constructive comments. Age dating of this study has been encouraged by a research project supported by Dokuz Eylül University (project numbers: 2009.KB.FEN.026).

Appendix 1. Results of Ar/Ar age dating in this study

Single crystal total fusion $^{40}Ar/^{39}Ar$ dating of the sample 116 [Yuntdağ volcanics] (mineral: biotite; N: 17).

Mineral	P (%)	t	40 V	39 V	38 V	37 V	36 V	Moles $^{40}Ar^*$	%Rad	R	Age (Ma)	%-sd
a	1.8	10	3.65597 ± 0.00441	2.09289 ± 0.00102	0.03094 ± 0.00020	0.03527 ± 0.00043	0.000965 ± 0.00002	2.56E−14	92.28%	1.6120	18.77 ± 0.05	0.25%
b	1.8	10	2.04824 ± 0.00216	1.18621 ± 0.00191	0.01749 ± 0.00022	0.05343 ± 0.00023	0.000484 ± 0.00002	1.43E−14	93.23%	1.6099	18.74 ± 0.07	0.35%
c	1.8	10	1.75650 ± 0.00147	1.00735 ± 0.00201	0.01476 ± 0.00018	0.01363 ± 0.00030	0.000463 ± 0.00002	1.23E−14	92.27%	1.6090	18.73 ± 0.08	0.45%
d	1.8	10	2.50708 ± 0.00140	1.38935 ± 0.00116	0.02051 ± 0.00025	0.13572 ± 0.00152	0.000961 ± 0.00002	1.76E−14	89.12%	1.6083	18.72 ± 0.05	0.28%
e	1.8	10	1.04308 ± 0.00161	0.62061 ± 0.00083	0.00843 ± 0.00006	0.00146 ± 0.00012	0.000170 ± 0.00002	7.31E−15	95.20%	1.6001	18.63 ± 0.11	0.61%
f	1.8	10	2.74284 ± 0.00250	1.46303 ± 0.00145	0.02207 ± 0.00026	0.07064 ± 0.00084	0.001272 ± 0.00002	1.92E−14	86.51%	1.6220	18.88 ± 0.06	0.29%
g	1.8	10	2.43856 ± 0.00152	1.39063 ± 0.00106	0.02034 ± 0.00025	0.07017 ± 0.00079	0.000742 ± 0.00003	1.71E−14	91.25%	1.6001	18.63 ± 0.08	0.45%
h	1.8	10	2.00059 ± 0.00195	1.09523 ± 0.00156	0.01596 ± 0.00015	0.03292 ± 0.00034	0.000803 ± 0.00002	1.40E−14	88.27%	1.6124	18.77 ± 0.07	0.36%
i	1.8	10	1.50259 ± 0.00183	0.87188 ± 0.00141	0.01231 ± 0.00009	0.01489 ± 0.00019	0.000341 ± 0.00002	1.05E−14	93.37%	1.6092	18.74 ± 0.09	0.49%
j	1.8	10	1.17484 ± 0.00082	0.68702 ± 0.00081	0.01004 ± 0.00011	0.03328 ± 0.00074	0.000253 ± 0.00002	8.23E−15	93.86%	1.6051	18.69 ± 0.09	0.50%
k	1.8	10	0.67233 ± 0.00072	0.36952 ± 0.00054	0.00558 ± 0.00012	0.00677 ± 0.00015	0.000264 ± 0.00002	4.71E−15	88.49%	1.6102	18.75 ± 0.17	0.90%
l	1.8	10	0.93604 ± 0.00124	0.52416 ± 0.00066	0.00773 ± 0.00012	0.02810 ± 0.00044	0.000328 ± 0.00002	6.56E−15	89.91%	1.6056	18.69 ± 0.12	0.64%
m	1.8	10	1.40696 ± 0.00134	0.79140 ± 0.00119	0.01140 ± 0.00012	0.00664 ± 0.00023	0.000415 ± 0.00002	9.85E−15	91.33%	1.6237	18.90 ± 0.09	0.47%
n	1.8	10	5.06628 ± 0.00257	2.91617 ± 0.00220	0.04246 ± 0.00026	0.06413 ± 0.00133	0.001278 ± 0.00003	3.55E−14	92.65%	1.6097	18.74 ± 0.04	0.23%
o	1.8	10	1.57449 ± 0.00178	0.83177 ± 0.00110	0.01231 ± 0.00015	0.01199 ± 0.00029	0.000788 ± 0.00002	1.10E−14	85.28%	1.6143	18.79 ± 0.09	0.48%
p	1.8	15	7.99304 ± 0.00569	4.13836 ± 0.00144	0.06205 ± 0.00045	0.13903 ± 0.00115	0.004402 ± 0.00006	5.60E−14	83.87%	1.6199	18.86 ± 0.05	0.29%
q	1.8	15	1.71527 ± 0.00201	0.99023 ± 0.00119	0.01487 ± 0.00024	0.08202 ± 0.00106	0.000408 ± 0.00002	1.20E−14	93.37%	1.6175	18.83 ± 0.07	0.35%

Single crystal incremental heating $^{40}Ar/^{39}Ar$ dating of the sample 116 [Yuntdağ volcanics] (mineral: biotite)

Steps	P (%)	t	40 V	39 V	38 V	37 V	36 V	Moles $^{40}Ar^*$	%Rad	R	Age (Ma)	%-sd
1	0.4	30	0.26848 ± 0.00058	0.01113 ± 0.00022	0.00033 ± 0.00004	0.00094 ± 0.00026	0.000803 ± 0.00002	1.88E−15	11.62%	2.8031	32.51 ± 9.21	28.34%
2	0.44	30	0.02315 ± 0.00040	0.00644 ± 0.00023	0.00015 ± 0.00004	−0.00003 ± 0.00011	0.000032 ± 0.00002	1.62E−16	59.25%	2.1298	24.75 ± 10.63	42.93%
3	0.48	20	0.01592 ± 0.00039	0.00618 ± 0.00014	0.00014 ± 0.00004	−0.00004 ± 0.00031	0.000003 ± 0.00003	1.11E−16	94.64%	2.4351	28.28 ± 18.96	67.06%
4	0.52	15	0.02319 ± 0.00047	0.00952 ± 0.00019	0.00018 ± 0.00005	−0.00019 ± 0.00008	−0.000002 ± 0.00002	1.62E−16	102.82%	2.4342	28.27 ± 7.58	26.82%
5	0.56	15	0.02827 ± 0.00047	0.01486 ± 0.00027	0.00021 ± 0.00004	−0.00001 ± 0.00024	0.000003 ± 0.00002	1.98E−16	96.38%	1.8335	21.33 ± 4.82	22.62%
6	0.6	15	0.04071 ± 0.00045	0.02045 ± 0.00024	0.00032 ± 0.00004	0.00018 ± 0.00018	0.000009 ± 0.00002	2.85E−16	93.43%	1.8600	21.64 ± 3.19	14.73%
7	0.65	15	0.06201 ± 0.00048	0.03511 ± 0.00016	0.00055 ± 0.00005	0.00006 ± 0.00024	0.000029 ± 0.00002	4.34E−16	85.99%	1.5186	17.69 ± 1.91	10.82%
8	0.72	15	0.14844 ± 0.00126	0.07997 ± 0.00038	0.00114 ± 0.00004	0.00306 ± 0.00022	0.000053 ± 0.00002	1.04E−15	89.56%	1.6624	19.35 ± 0.92	4.74%
9	0.8	15	0.28961 ± 0.00077	0.16721 ± 0.00039	0.00237 ± 0.00006	0.00963 ± 0.00023	0.000057 ± 0.00002	2.03E−15	94.41%	1.6353	19.04 ± 0.37	1.96%
10	0.9	15	0.67735 ± 0.00157	0.39790 ± 0.00089	0.00598 ± 0.00011	0.03294 ± 0.00027	0.000140 ± 0.00002	4.74E−15	94.31%	1.6055	18.69 ± 0.17	0.93%
11	1	15	1.38353 ± 0.00090	0.83060 ± 0.00100	0.01236 ± 0.00019	0.06228 ± 0.00082	0.000132 ± 0.00002	9.69E−15	97.55%	1.6249	18.92 ± 0.09	0.50%
12	1.1	15	1.64156 ± 0.00166	0.99911 ± 0.00130	0.01458 ± 0.00022	0.06314 ± 0.00094	0.000144 ± 0.00002	1.15E−14	97.73%	1.6058	18.70 ± 0.08	0.43%
13	1.2	15	1.33733 ± 0.00146	0.81718 ± 0.00093	0.01224 ± 0.00018	0.04067 ± 0.00053	0.000082 ± 0.00002	9.37E−15	98.45%	1.6111	18.76 ± 0.09	0.47%
14	1.4	15	0.70770 ± 0.00078	0.43315 ± 0.00085	0.00636 ± 0.00010	0.03499 ± 0.00069	0.000063 ± 0.00002	4.96E−15	97.78%	1.5976	18.60 ± 0.15	0.83%
15	1.6	15	0.10244 ± 0.00052	0.06093 ± 0.00024	0.00092 ± 0.00004	0.00212 ± 0.00017	−0.000039 ± 0.00003	7.17E−16	111.33%	1.6842	19.60 ± 1.84	9.40%

P: % power of 60 W (60 W *(P/10) Synrad CO_2 laser); t: laser duration time; V: volt; %Rad: % radiogenic argon; R: $^{40}Ar^*/^{39}Ar$ (Ar^*: radiogenic argon); J value: 0.0064870 ± 0.000011 (1σ).

Single crystal total fusion $^{40}Ar/^{39}Ar$ dating of the sample 128 (mineral: biotite; N: 19)

Minerals	P (%)	t	40 V	39 V	38 V	37 V	36 V	Moles $^{40}Ar^{*}$	%Rad	R	Age (Ma)	%-sd
a	1.8	15	2.21580 ± 0.00197	0.78234 ± 0.00144	0.01202 ± 0.00018	0.01484 ± 0.00032	0.002940 ± 0.00005	1.55E−14	60.85%	1.7234	20.06 ± 0.25	1.24%
b	1.8	15	2.21580 ± 0.00197	0.78234 ± 0.00144	0.01202 ± 0.00018	0.01484 ± 0.00032	0.002940 ± 0.00005	1.55E−14	60.85%	1.7234	20.06 ± 0.25	1.24%
c	1.8	15	8.37854 ± 0.00795	4.23865 ± 0.00188	0.06139 ± 0.00019	0.12152 ± 0.00105	0.003883 ± 0.00003	5.87E−14	86.42%	1.7084	19.88 ± 0.04	0.18%
d	1.8	10	4.20839 ± 0.00293	2.14468 ± 0.00230	0.03102 ± 0.00023	0.06027 ± 0.00114	0.001842 ± 0.00003	2.95E−14	87.19%	1.7108	19.91 ± 0.05	0.25%
e	1.8	10	5.00677 ± 0.00411	1.10546 ± 0.00188	0.01795 ± 0.00016	0.01901 ± 0.00019	0.010467 ± 0.00010	3.51E−14	38.25%	1.7326	20.16 ± 0.32	1.59%
f	1.8	10	1.25408 ± 0.00105	0.65075 ± 0.00108	0.00944 ± 0.00014	0.00948 ± 0.00017	0.000485 ± 0.00002	8.78E−15	88.63%	1.7081	19.88 ± 0.12	0.62%
*g	1.8	10	2.08429 ± 0.00249	0.85629 ± 0.00103	0.01273 ± 0.00018	0.02290 ± 0.00030	0.001959 ± 0.00002	1.46E−14	72.31%	1.7602	20.48 ± 0.11	0.52%
h	1.8	10	2.41676 ± 0.00297	1.19844 ± 0.00081	0.01762 ± 0.00011	0.09178 ± 0.00139	0.001247 ± 0.00002	1.69E−14	85.07%	1.7156	19.97 ± 0.08	0.40%
i	1.8	10	4.59725 ± 0.00389	1.71227 ± 0.00189	0.02578 ± 0.00014	0.06594 ± 0.00050	0.005514 ± 0.00003	3.22E−14	64.67%	1.7365	20.21 ± 0.08	0.41%
j	1.8	10	1.80616 ± 0.00130	0.82382 ± 0.00081	0.01256 ± 0.00011	0.13135 ± 0.00103	0.001395 ± 0.00003	1.26E−14	77.78%	1.7055	19.85 ± 0.11	0.56%
k	*1.8*	*10*	*1.24707 ± 0.00110*	*0.41993 ± 0.00044*	*0.00606 ± 0.00007*	*0.01532 ± 0.00033*	*0.001721 ± 0.00002*	*8.73E−15*	*59.32%*	*1.7617*	*20.50 ± 0.19*	*0.92%*
l	*1.8*	*10*	*1.43191 ± 0.00153*	*0.76881 ± 0.00111*	*0.01073 ± 0.00010*	*0.01446 ± 0.00016*	*0.000402 ± 0.00002*	*1.00E−14*	*91.79%*	*1.7097*	*19.90 ± 0.09*	*0.47%*
m	1.8	10	2.66413 ± 0.00398	1.45923 ± 0.00147	0.02102 ± 0.00022	0.04155 ± 0.00046	0.000638 ± 0.00002	1.87E−14	93.05%	1.6989	19.77 ± 0.06	0.32%
n	1.8	10	2.70768 ± 0.00143	1.47569 ± 0.00167	0.02136 ± 0.00021	0.06336 ± 0.00066	0.000665 ± 0.00002	1.90E−14	92.94%	1.7053	19.85 ± 0.06	0.28%
o	1.8	15	1.76729 ± 0.00184	0.95027 ± 0.00099	0.01401 ± 0.00013	0.02182 ± 0.00032	0.000507 ± 0.00002	1.24E−14	91.62%	1.7040	19.83 ± 0.09	0.43%
p	1.8	15	1.90751 ± 0.00298	1.05286 ± 0.00097	0.01523 ± 0.00010	0.01804 ± 0.00037	0.000388 ± 0.00002	1.34E−14	94.06%	1.7042	19.84 ± 0.08	0.40%
q	1.8	15	2.19020 ± 0.00134	0.65353 ± 0.00102	0.01028 ± 0.00018	0.01047 ± 0.00032	0.003624 ± 0.00004	1.53E−14	51.15%	1.7143	19.95 ± 0.22	1.09%
r	2	10	2.45356 ± 0.00268	1.14194 ± 0.00135	0.01671 ± 0.00016	0.01363 ± 0.00024	0.001644 ± 0.00002	1.72E−14	80.25%	1.7242	20.07 ± 0.08	0.40%
s	2	10	1.79279 ± 0.00193	0.80288 ± 0.00113	0.01165 ± 0.00013	0.01130 ± 0.00018	0.001369 ± 0.00003	1.26E−14	77.49%	1.7302	20.14 ± 0.12	0.59%

Single crystal incremental heating $^{40}Ar/^{39}Ar$ dating of the sample 118 (mineral: biotite)

Steps	P (%)	t	40 V	39 V	38 V	37 V	36 V	Moles $^{40}Ar^{*}$	%Rad	R	Age (Ma)	%-sd
1	0.4	30	0.99350 ± 0.00113	0.00258 ± 0.00016	0.00061 ± 0.00005	0.00063 ± 0.00027	0.003248 ± 0.00003	6.96E−15	3.39%	13.0572	146.68 ± 383.79	261.65%
2	0.44	30	0.21458 ± 0.00077	0.00258 ± 0.00015	0.00011 ± 0.00005	0.00029 ± 0.00025	0.000651 ± 0.00002	1.50E−15	10.36%	8.6211	98.17 ± 78.64	80.10%
3	0.48	20	0.02905 ± 0.00055	0.00226 ± 0.00017	−0.00020 ± 0.00008	0.00086 ± 0.00016	0.000085 ± 0.00002	2.03E−16	13.59%	1.7508	20.37 ± 30.32	148.82%
4	0.52	15	0.01143 ± 0.00051	0.00243 ± 0.00017	0.00000 ± 0.00004	0.00054 ± 0.00019	0.000021 ± 0.00002	8.00E−17	47.01%	2.2076	25.65 ± 23.61	92.05%
5	0.56	15	0.03170 ± 0.00054	0.00666 ± 0.00021	0.00000 ± 0.00005	0.00028 ± 0.00009	0.000074 ± 0.00002	2.22E−16	31.34%	1.4913	17.37 ± 9.31	53.60%
6	0.6	15	0.04759 ± 0.00059	0.01478 ± 0.00030	0.00020 ± 0.00006	0.00054 ± 0.00015	0.000074 ± 0.00002	3.33E−16	54.06%	1.7411	20.26 ± 4.64	22.90%
7	0.65	15	0.12162 ± 0.00064	0.03837 ± 0.00018	0.00049 ± 0.00004	0.00091 ± 0.00017	0.000163 ± 0.00002	8.52E−16	60.46%	1.9165	22.29 ± 1.59	7.15%
8	0.72	15	0.13913 ± 0.00049	0.07001 ± 0.00042	0.00092 ± 0.00005	0.00179 ± 0.00012	0.000057 ± 0.00002	9.74E−16	87.96%	1.7482	20.34 ± 0.90	4.43%
9	0.8	15	0.20373 ± 0.00069	0.10582 ± 0.00046	0.00149 ± 0.00005	0.00254 ± 0.00021	0.000094 ± 0.00002	1.43E−15	86.52%	1.6659	19.39 ± 0.51	2.63%
10	0.9	15	0.45650 ± 0.00061	0.24568 ± 0.00063	0.00333 ± 0.00006	0.00858 ± 0.00019	0.000131 ± 0.00002	3.20E−15	91.70%	1.7040	19.83 ± 0.28	1.42%
11	1	15	0.89258 ± 0.00094	0.51000 ± 0.00071	0.00737 ± 0.00012	0.02067 ± 0.00034	−0.000014 ± 0.00003	6.25E−15	100.66%	1.7536	20.41 ± 0.19	0.95%
12	1.1	15	1.27670 ± 0.00094	0.73676 ± 0.00072	0.01017 ± 0.00009	0.03048 ± 0.00044	0.000090 ± 0.00002	8.94E−15	98.12%	1.7003	19.79 ± 0.08	0.41%
13	1.2	15	1.68951 ± 0.00194	0.98397 ± 0.00123	0.01416 ± 0.00016	0.03049 ± 0.00029	0.000082 ± 0.00002	1.18E−14	98.72%	1.6952	19.73 ± 0.07	0.35%
14	1.4	15	2.35114 ± 0.00460	1.37107 ± 0.00136	0.01971 ± 0.00009	0.03490 ± 0.00040	0.000092 ± 0.00002	1.65E−14	98.97%	1.6972	19.75 ± 0.07	0.34%
15	1.6	15	2.82956 ± 0.00186	1.64421 ± 0.00186	0.02354 ± 0.00031	0.03482 ± 0.00071	0.000151 ± 0.00002	1.98E−14	98.53%	1.6957	19.74 ± 0.05	0.25%
16	1.7	15	0.03637 ± 0.00033	0.01507 ± 0.00016	0.00021 ± 0.00004	0.00796 ± 0.00026	0.000034 ± 0.00002	2.55E−16	74.02%	1.7870	20.79 ± 4.56	21.93%
17	1.8	15	0.00369 ± 0.00021	0.00117 ± 0.00013	−0.00003 ± 0.00004	0.00039 ± 0.00024	−0.000022 ± 0.00002	2.58E−17	277.89%	3.1800	36.84 ± 55.30	150.12%
18	2	15	0.00006 ± 0.00029	0.00009 ± 0.00011	−0.00004 ± 0.00003	0.00042 ± 0.00017	−0.000015 ± 0.00002	4.42E−19	7398.35%	1.0149	11.84 ± 921.91	7787.23%

(continued on next page)

Appendix 1 (*continued*)

Whole rock incremental heating $^{40}Ar/^{39}Ar$ dating of the sample 124 [Adilköy basalt]

Steps	P (%)	t	40 V	39 V	38 V	37 V	36 V	Moles $^{40}Ar^{*}$	%Rad	R	Age (Ma)	%-sd
1	0.5	30	0.08017 ± 0.00039	0.00153 ± 0.00011	0.00013 ± 0.00004	0.00034 ± 0.00190	0.000230 ± 0.00002	5.61E−16	15.26%	8.0221	91.52 ± 68.23	74.55%
2	0.6	30	0.67809 ± 0.00110	0.01223 ± 0.00011	0.00062 ± 0.00004	0.01655 ± 0.00262	0.001881 ± 0.00002	4.75E−15	18.24%	10.1280	114.80 ± 9.16	7.98%
3	0.7	30	0.51426 ± 0.00121	0.00952 ± 0.00011	0.00049 ± 0.00004	0.00867 ± 0.00131	0.001380 ± 0.00002	3.60E−15	20.86%	11.2686	127.28 ± 11.92	9.37%
4	0.75	30	1.80383 ± 0.00118	0.04239 ± 0.00018	0.00162 ± 0.00005	0.05260 ± 0.00240	0.004960 ± 0.00005	1.26E−14	18.99%	8.0883	92.26 ± 5.04	5.47%
5	0.8	30	1.69816 ± 0.00194	0.06879 ± 0.00028	0.00182 ± 0.00004	0.07739 ± 0.00368	0.004321 ± 0.00005	1.19E−14	25.18%	6.2219	71.38 ± 2.98	4.17%
6	0.85	30	1.33009 ± 0.00197	0.08422 ± 0.00028	0.00172 ± 0.00005	0.10424 ± 0.00146	0.003268 ± 0.00005	9.32E−15	28.06%	4.4350	51.17 ± 2.16	4.21%
7	1	30	2.23015 ± 0.00223	0.18442 ± 0.00046	0.00353 ± 0.00007	0.21710 ± 0.00307	0.005208 ± 0.00006	1.56E−14	31.80%	3.8489	44.49 ± 1.26	2.83%
8	1.15	30	2.84598 ± 0.00374	0.30460 ± 0.00060	0.00501 ± 0.00006	0.38203 ± 0.00633	0.006257 ± 0.00007	1.99E−14	36.15%	3.3809	39.14 ± 0.79	2.02%
9	1.3	30	2.41688 ± 0.00260	0.40444 ± 0.00083	0.00572 ± 0.00008	0.49831 ± 0.00400	0.004663 ± 0.00005	1.69E−14	44.70%	2.6738	31.02 ± 0.47	1.51%
10	1.45	30	1.61993 ± 0.00205	0.40598 ± 0.00076	0.00570 ± 0.00008	0.41842 ± 0.00355	0.002652 ± 0.00005	1.13E−14	53.76%	2.1467	24.95 ± 0.44	1.76%
11	1.6	30	1.16569 ± 0.00125	0.33277 ± 0.00055	0.00439 ± 0.00007	0.34830 ± 0.00383	0.001685 ± 0.00002	8.16E−15	59.76%	2.0951	24.35 ± 0.22	0.89%
12	1.75	30	1.67144 ± 0.00128	0.61491 ± 0.00110	0.00840 ± 0.00008	0.54648 ± 0.00807	0.001757 ± 0.00002	1.17E−14	71.66%	1.9491	22.67 ± 0.14	0.61%
13	1.9	30	0.50468 ± 0.00066	0.23348 ± 0.00051	0.00305 ± 0.00004	0.23554 ± 0.00402	0.000370 ± 0.00002	3.53E−15	82.20%	1.7781	20.69 ± 0.30	1.43%
14	2.05	30	0.27300 ± 0.00050	0.12969 ± 0.00059	0.00172 ± 0.00004	0.13071 ± 0.00117	0.000191 ± 0.00002	1.91E−15	83.25%	1.7539	20.41 ± 0.50	2.43%
15	2.2	30	0.45594 ± 0.00073	0.21154 ± 0.00044	0.00284 ± 0.00005	0.51687 ± 0.01199	0.000453 ± 0.00002	3.19E−15	80.03%	1.7280	20.11 ± 0.28	1.39%
16	2.35	30	0.12301 ± 0.00039	0.05753 ± 0.00024	0.00076 ± 0.00004	0.43224 ± 0.00796	0.000198 ± 0.00002	8.61E−16	81.58%	1.7542	20.41 ± 1.29	6.30%
17	2.5	30	0.17803 ± 0.00042	0.08246 ± 0.00040	0.00114 ± 0.00004	0.42459 ± 0.00568	0.000224 ± 0.00003	1.25E−15	82.65%	1.7913	20.84 ± 1.12	5.40%
18	2.8	30	0.09939 ± 0.00045	0.03826 ± 0.00024	0.00055 ± 0.00003	0.50634 ± 0.00377	0.000211 ± 0.00004	6.96E−16	79.59%	2.0884	24.28 ± 3.16	13.03%
19	3	30	0.02461 ± 0.00033	0.00926 ± 0.00014	0.00022 ± 0.00004	0.18828 ± 0.00295	0.000114 ± 0.00002	1.72E−16	26.80%	0.7233	8.44 ± 6.08	72.00%
20	3.3	30	0.01128 ± 0.00030	0.00407 ± 0.00013	−0.00002 ± 0.00006	0.13989 ± 0.00088	0.000028 ± 0.00003	7.90E−17	129.79%	3.6925	42.70 ± 27.36	64.06%

Whole rock incremental heating $^{40}Ar/^{39}Ar$ dating of the sample 911 [Adilköy basalt]

Steps	P (%)	t	40 V	39 V	38 V	37 V	36 V	Moles $^{40}Ar^{*}$	%Rad	R	Age (Ma)	%-sd
1	0.6	30	1.86934 ± 0.00162	0.01354 ± 0.00016	0.00138 ± 0.00003	0.00916 ± 0.00149	0.006240 ± 0.00007	1.31E−14	1.40%	1.9376	22.53 ± 32.56	144.48%
2	0.7	30	2.24543 ± 0.00227	0.02877 ± 0.00014	0.00179 ± 0.00006	0.02774 ± 0.00134	0.007296 ± 0.00005	1.57E−14	4.09%	3.1964	37.03 ± 8.83	23.84%
3	0.75	30	1.43331 ± 0.00175	0.04330 ± 0.00029	0.00145 ± 0.00004	0.05574 ± 0.00203	0.004399 ± 0.00006	1.00E−14	9.62%	3.1873	36.92 ± 6.15	16.67%
4	0.85	30	0.97426 ± 0.00104	0.06156 ± 0.00045	0.00139 ± 0.00003	0.10929 ± 0.00148	0.002764 ± 0.00004	6.82E−15	17.09%	2.7074	31.41 ± 2.86	9.12%
5	0.9	30	0.69198 ± 0.00121	0.06739 ± 0.00040	0.00121 ± 0.00004	0.12884 ± 0.00265	0.001824 ± 0.00003	4.85E−15	23.67%	2.4341	28.26 ± 1.58	5.57%
6	1	30	0.74789 ± 0.00105	0.10002 ± 0.00048	0.00162 ± 0.00005	0.21893 ± 0.00329	0.001836 ± 0.00002	5.24E−15	29.89%	2.2387	26.01 ± 0.92	3.52%
7	1.15	30	1.07810 ± 0.00661	0.21628 ± 0.00046	0.00323 ± 0.00008	0.51933 ± 0.00843	0.002373 ± 0.00002	7.55E−15	38.94%	1.9448	22.62 ± 0.55	2.41%
8	1.2	30	0.53885 ± 0.00095	0.14248 ± 0.00030	0.00201 ± 0.00006	0.28292 ± 0.00712	0.000918 ± 0.00002	3.77E−15	54.03%	2.0462	23.79 ± 0.58	2.43%
9	1.45	30	1.07854 ± 0.00122	0.43443 ± 0.00108	0.00555 ± 0.00006	0.54064 ± 0.00822	0.000970 ± 0.00002	7.55E−15	77.60%	1.9282	22.43 ± 0.20	0.89%
10	1.55	30	1.06962 ± 0.00119	0.49237 ± 0.00081	0.00613 ± 0.00005	0.36977 ± 0.00382	0.000687 ± 0.00002	7.49E−15	83.89%	1.8235	21.21 ± 0.14	0.68%
11	1.65	30	0.99239 ± 0.00152	0.44653 ± 0.00066	0.00579 ± 0.00008	0.33732 ± 0.00343	0.000768 ± 0.00004	6.95E−15	79.94%	1.7777	20.69 ± 0.28	1.37%
12	1.75	30	0.66948 ± 0.00112	0.29477 ± 0.00051	0.00383 ± 0.00008	0.23830 ± 0.00322	0.000546 ± 0.00001	4.69E−15	78.86%	1.7921	20.85 ± 0.18	0.85%
13	1.9	30	1.13391 ± 0.00123	0.49635 ± 0.00103	0.00681 ± 0.00013	0.53815 ± 0.00822	0.000984 ± 0.00002	7.94E−15	78.30%	1.7901	20.83 ± 0.17	0.82%
14	2.1	30	0.44142 ± 0.00092	0.18430 ± 0.00031	0.00232 ± 0.00006	0.19622 ± 0.00257	0.000439 ± 0.00002	3.09E−15	74.31%	1.7812	20.73 ± 0.37	1.77%
15	2.35	30	0.58148 ± 0.00231	0.24748 ± 0.00046	0.00322 ± 0.00005	0.42558 ± 0.00540	0.000633 ± 0.00002	4.07E−15	73.89%	1.7383	20.23 ± 0.31	1.52%
16	2.5	30	0.33956 ± 0.00075	0.12040 ± 0.00041	0.00162 ± 0.00005	0.66624 ± 0.00836	0.000621 ± 0.00002	2.38E−15	62.23%	1.7623	20.51 ± 0.62	3.02%
17	2.65	30	0.29001 ± 0.00051	0.09861 ± 0.00027	0.00135 ± 0.00005	0.66014 ± 0.01055	0.000597 ± 0.00002	2.03E−15	58.06%	1.7163	19.97 ± 0.73	3.67%
18	2.8	30	0.14616 ± 0.00039	0.04886 ± 0.00029	0.00067 ± 0.00003	0.32476 ± 0.00455	0.000302 ± 0.00002	1.02E−15	57.42%	1.7262	20.09 ± 1.33	6.64%
19	3	30	0.13005 ± 0.00035	0.04449 ± 0.00024	0.00063 ± 0.00004	0.24870 ± 0.00376	0.000226 ± 0.00002	9.11E−16	64.57%	1.8953	22.05 ± 1.25	5.66%
20	3.3	30	0.30047 ± 0.00047	0.06610 ± 0.00033	0.00097 ± 0.00005	0.91991 ± 0.00934	0.000896 ± 0.00002	2.10E−15	37.28%	1.7124	19.93 ± 0.98	4.90%
21	3.5	30	0.03894 ± 0.00037	0.00947 ± 0.00014	0.00016 ± 0.00004	0.14752 ± 0.00376	0.000144 ± 0.00002	2.73E−16	21.88%	0.9105	10.62 ± 6.05	56.95%

Whole rock incremental heating $^{40}Ar/^{39}Ar$ dating of the sample 115 [Yuntdağ volcanics]

Sample	P (%)	t	40 V	39 V	38 V	37 V	36 V	Moles $^{40}Ar^{*}$	%Rad	R	Age (Ma)	%-sd
1	0.4	30	1.02095 ± 0.00199	0.00128 ± 0.00019	0.00063 ± 0.00008	0.00175 ± 0.00162	0.003285 ± 0.00004	7.15E−15	4.94%	39.3558	410.20 ± 1721.36	419.64%
2	0.5	30	5.79549 ± 0.00765	0.02177 ± 0.00028	0.00391 ± 0.00008	0.03001 ± 0.00093	0.018519 ± 0.00009	4.06E−14	5.62%	14.9715	167.22 ± 54.11	32.36%
3	0.6	30	5.57044 ± 0.00674	0.09093 ± 0.00025	0.00494 ± 0.00010	0.17389 ± 0.00139	0.017501 ± 0.00010	3.90E−14	7.42%	4.5534	52.52 ± 4.71	8.97%
4	0.7	30	4.21919 ± 0.00353	0.16876 ± 0.00034	0.00492 ± 0.00009	0.31092 ± 0.00199	0.012761 ± 0.00008	2.95E−14	11.24%	2.8141	32.64 ± 1.84	5.64%
5	0.8	30	3.12798 ± 0.00297	0.31025 ± 0.00099	0.00568 ± 0.00009	0.52026 ± 0.00249	0.008821 ± 0.00009	2.19E−14	18.05%	1.8218	21.20 ± 1.14	5.39%
6	0.9	30	2.89173 ± 0.00292	0.71586 ± 0.00082	0.01008 ± 0.00014	1.02952 ± 0.00490	0.005519 ± 0.00004	2.03E−14	46.56%	1.8827	21.90 ± 0.21	0.98%

7	0.95	30	0.76388 ± 0.00090	0.23737 ± 0.00082	0.00306 ± 0.00007	0.29226 ± 0.00302	0.001247 ± 0.00003	5.35E−15	54.95%	1.7701	20.60 ± 0.53	2.56%
8	1	30	0.50183 ± 0.00087	0.15916 ± 0.00056	0.00205 ± 0.00008	0.19282 ± 0.00233	0.000784 ± 0.00003	3.51E−15	57.04%	1.8000	20.94 ± 0.73	3.47%
9	1.05	30	0.48291 ± 0.00039	0.15615 ± 0.00043	0.00205 ± 0.00008	0.18885 ± 0.00216	0.000726 ± 0.00004	3.38E−15	58.80%	1.8202	21.18 ± 0.81	3.85%
10	1.1	30	0.48922 ± 0.00101	0.15964 ± 0.00054	0.00215 ± 0.00008	0.19000 ± 0.00227	0.000816 ± 0.00004	3.43E−15	53.96%	1.6549	19.26 ± 0.82	4.25%
11	1.15	30	0.58198 ± 0.00093	0.18723 ± 0.00053	0.00255 ± 0.00009	0.20675 ± 0.00108	0.000892 ± 0.00003	4.08E−15	57.68%	1.7944	20.88 ± 0.64	3.07%
12	1.2	30	0.51221 ± 0.00108	0.16529 ± 0.00054	0.00217 ± 0.00007	0.17043 ± 0.00161	0.000846 ± 0.00004	3.59E−15	53.96%	1.6733	19.48 ± 0.89	4.57%
13	1.25	30	0.53945 ± 0.00095	0.16934 ± 0.00050	0.00198 ± 0.00010	0.16713 ± 0.00098	0.000829 ± 0.00004	3.78E−15	57.16%	1.8223	21.20 ± 0.77	3.61%
14	1.3	30	0.76486 ± 0.00129	0.24801 ± 0.00064	0.00337 ± 0.00012	0.23083 ± 0.00235	0.001176 ± 0.00004	5.36E−15	57.06%	1.7609	20.49 ± 0.60	2.91%
15	1.35	30	1.25695 ± 0.00087	0.43049 ± 0.00101	0.00570 ± 0.00009	0.36442 ± 0.00279	0.001802 ± 0.00003	8.80E−15	60.05%	1.7543	20.42 ± 0.28	1.37%
16	1.4	30	0.64984 ± 0.00221	0.20927 ± 0.00067	0.00282 ± 0.00009	0.15665 ± 0.00148	0.000998 ± 0.00004	4.55E−15	56.61%	1.7587	20.47 ± 0.64	3.13%
17	1.45	30	0.77770 ± 0.00080	0.24580 ± 0.00026	0.00337 ± 0.00007	0.18296 ± 0.00113	0.001255 ± 0.00003	5.45E−15	54.25%	1.7173	19.99 ± 0.43	2.16%
18	1.5	30	1.44676 ± 0.00157	0.46723 ± 0.00058	0.00629 ± 0.00010	0.42894 ± 0.00201	0.002303 ± 0.00004	1.01E−14	55.43%	1.7174	19.99 ± 0.30	1.50%
19	1.55	30	1.39537 ± 0.00099	0.43808 ± 0.00052	0.00633 ± 0.00010	0.42276 ± 0.00424	0.002234 ± 0.00004	9.77E−15	55.21%	1.7600	20.48 ± 0.29	1.40%
20	1.6	30	1.03554 ± 0.00155	0.29542 ± 0.00047	0.00412 ± 0.00008	0.34709 ± 0.00381	0.001847 ± 0.00003	7.25E−15	50.08%	1.7569	20.44 ± 0.39	1.89%
21	1.65	30	0.44843 ± 0.00063	0.11398 ± 0.00024	0.00163 ± 0.00007	0.12072 ± 0.00106	0.000908 ± 0.00003	3.14E−15	42.40%	1.6695	19.43 ± 1.02	5.27%
22	1.75	30	0.68036 ± 0.00104	0.16771 ± 0.00045	0.00243 ± 0.00010	0.23862 ± 0.00285	0.001347 ± 0.00004	4.76E−15	44.39%	1.8028	20.98 ± 0.78	3.73%
23	1.9	30	0.53231 ± 0.00092	0.12401 ± 0.00048	0.00171 ± 0.00008	0.18666 ± 0.00080	0.001074 ± 0.00003	3.73E−15	43.30%	1.8607	21.65 ± 0.95	4.41%
24	2.1	15	0.26739 ± 0.00064	0.06090 ± 0.00037	0.00089 ± 0.00006	0.10612 ± 0.00121	0.000557 ± 0.00004	1.87E−15	41.76%	1.8360	21.36 ± 2.12	9.95%
25	2.3	15	0.34302 ± 0.00082	0.07679 ± 0.00032	0.00116 ± 0.00007	0.14400 ± 0.00120	0.000735 ± 0.00003	2.40E−15	40.18%	1.7973	20.91 ± 1.40	6.69%
26	2.5	15	0.21395 ± 0.00084	0.04551 ± 0.00019	0.00074 ± 0.00007	0.10183 ± 0.00104	0.000478 ± 0.00003	1.50E−15	37.99%	1.7887	20.81 ± 2.59	12.46%
27	2.9	20	0.86498 ± 0.00109	0.18717 ± 0.00039	0.00283 ± 0.00010	0.47929 ± 0.00363	0.001891 ± 0.00004	6.06E−15	40.00%	1.8523	21.41 ± 0.67	3.15%
28	3	15	0.16064 ± 0.00049	0.03255 ± 0.00022	0.00052 ± 0.00004	0.05987 ± 0.00074	0.000387 ± 0.00003	1.12E−15	31.83%	1.5728	18.31 ± 3.56	19.43%
29	3.1	15	0.10100 ± 0.00040	0.01915 ± 0.00020	0.00015 ± 0.00006	0.03915 ± 0.00064	0.000247 ± 0.00004	7.07E−16	31.06%	1.6410	19.10 ± 6.75	35.35%

Whole rock incremental heating $^{40}Ar/^{39}Ar$ dating of the sample 915 [Dededağ volcanics]

Sample	P (%)	t	40 V	39 V	38 V	37 V	36 V	Moles $^{40}Ar^{*}$	%Rad	R	Age (Ma)	%-sd
1	0.4	30	0.06494 ± 0.00038	0.00299 ± 0.00018	0.00011 ± 0.00008	0.00607 ± 0.00097	0.000147 ± 0.00003	4.55E−16	33.77%	7.3550	84.09 ± 40.49	48.15%
2	0.5	30	0.43023 ± 0.00067	0.02565 ± 0.00026	0.00055 ± 0.00007	0.06702 ± 0.00079	0.001288 ± 0.00003	3.01E−15	12.82%	2.1543	25.04 ± 4.85	19.36%
3	0.6	30	1.47217 ± 0.00147	0.15075 ± 0.00017	0.00270 ± 0.00008	0.15290 ± 0.00110	0.003962 ± 0.00004	1.03E−14	21.33%	2.0842	24.23 ± 0.94	3.88%
4	0.65	30	1.30169 ± 0.00142	0.21395 ± 0.00064	0.00345 ± 0.00006	0.17485 ± 0.00129	0.003078 ± 0.00003	9.12E−15	31.23%	1.9014	22.12 ± 0.61	2.75%
5	0.7	30	1.50471 ± 0.00185	0.30694 ± 0.00040	0.00472 ± 0.00007	0.27491 ± 0.00172	0.003302 ± 0.00005	1.05E−14	36.67%	1.7991	20.93 ± 0.53	2.51%
6	0.76	30	1.47676 ± 0.00215	0.32992 ± 0.00065	0.00494 ± 0.00010	0.41831 ± 0.00254	0.003069 ± 0.00004	1.03E−14	40.95%	1.8345	21.34 ± 0.42	1.95%
7	0.82	30	1.60309 ± 0.00170	0.40584 ± 0.00067	0.00614 ± 0.00009	0.76740 ± 0.00496	0.003205 ± 0.00004	1.12E−14	44.90%	1.7762	20.67 ± 0.35	1.70%
8	0.9	30	1.87223 ± 0.00175	0.50901 ± 0.00100	0.00738 ± 0.00009	1.28795 ± 0.00531	0.003723 ± 0.00004	1.31E−14	46.95%	1.7301	20.13 ± 0.29	1.45%
9	0.95	30	1.71474 ± 0.00186	0.56408 ± 0.00045	0.00843 ± 0.00012	1.31979 ± 0.00915	0.002895 ± 0.00004	1.20E−14	56.50%	1.7204	20.02 ± 0.28	1.39%
10	1	30	0.95390 ± 0.00107	0.39010 ± 0.00049	0.00546 ± 0.00007	0.66868 ± 0.00362	0.001131 ± 0.00004	6.68E−15	70.80%	1.7334	20.17 ± 0.39	1.93%
11	1.05	30	0.91224 ± 0.00164	0.39021 ± 0.00077	0.00556 ± 0.00009	0.64411 ± 0.00309	0.001034 ± 0.00004	6.39E−15	72.38%	1.6942	19.72 ± 0.38	1.95%
12	1.1	30	0.97182 ± 0.00135	0.39208 ± 0.00051	0.00555 ± 0.00009	0.73104 ± 0.00369	0.001202 ± 0.00004	6.81E−15	69.71%	1.7303	20.14 ± 0.38	1.91%
13	1.15	30	0.78795 ± 0.00075	0.33021 ± 0.00063	0.00465 ± 0.00008	0.62388 ± 0.00269	0.000943 ± 0.00004	5.52E−15	71.19%	1.7012	19.80 ± 0.43	2.17%
14	1.2	30	0.60313 ± 0.00112	0.26825 ± 0.00049	0.00374 ± 0.00009	0.48437 ± 0.00116	0.000628 ± 0.00004	4.22E−15	75.88%	1.7084	19.88 ± 0.55	2.75%
15	1.25	30	0.24430 ± 0.00049	0.12240 ± 0.00062	0.00182 ± 0.00006	0.21292 ± 0.00240	0.000194 ± 0.00004	1.71E−15	83.83%	1.6754	19.50 ± 1.19	6.12%
16	1.3	30	0.27867 ± 0.00033	0.13482 ± 0.00037	0.00193 ± 0.00007	0.25826 ± 0.00210	0.000197 ± 0.00003	1.95E−15	86.77%	1.7961	20.90 ± 0.83	3.99%
17	1.35	30	0.33656 ± 0.00054	0.15618 ± 0.00039	0.00229 ± 0.00010	0.30838 ± 0.00306	0.000301 ± 0.00004	2.36E−15	81.17%	1.7516	20.38 ± 0.78	3.81%
18	1.4	30	0.35457 ± 0.00056	0.15754 ± 0.00041	0.00231 ± 0.00007	0.33506 ± 0.00337	0.000418 ± 0.00004	2.48E−15	72.99%	1.6453	19.15 ± 0.90	4.70%
19	1.45	30	0.34274 ± 0.00056	0.15366 ± 0.00047	0.00223 ± 0.00009	0.35055 ± 0.00177	0.000383 ± 0.00004	2.40E−15	75.46%	1.6860	19.62 ± 0.82	4.18%
20	1.5	30	0.12630 ± 0.00049	0.05947 ± 0.00033	0.00095 ± 0.00008	0.10070 ± 0.00115	0.000094 ± 0.00003	8.85E−16	84.69%	1.8009	20.95 ± 1.98	9.45%
21	1.57	30	0.16572 ± 0.00044	0.06544 ± 0.00028	0.00097 ± 0.00006	0.12001 ± 0.00180	0.000232 ± 0.00004	1.16E−15	64.56%	1.6373	19.06 ± 2.10	11.04%
22	1.64	30	0.23141 ± 0.00206	0.11076 ± 0.00039	0.00160 ± 0.00008	0.23584 ± 0.00131	0.000235 ± 0.00004	1.62E−15	78.45%	1.6416	19.11 ± 1.22	6.36%
23	1.7	30	0.31821 ± 0.00052	0.12460 ± 0.00039	0.00188 ± 0.00005	0.30446 ± 0.00256	0.000509 ± 0.00004	2.23E−15	60.70%	1.5531	18.08 ± 1.08	5.95%
24	1.77	30	0.21258 ± 0.00065	0.10852 ± 0.00042	0.00164 ± 0.00010	0.26511 ± 0.00229	0.000197 ± 0.00004	1.49E−15	82.90%	1.6270	18.94 ± 1.18	6.22%
25	1.84	30	0.23798 ± 0.00072	0.11536 ± 0.00048	0.00174 ± 0.00006	0.30799 ± 0.00322	0.000270 ± 0.00004	1.67E−15	77.24%	1.5965	18.59 ± 1.27	6.85%
26	2	15	0.04795 ± 0.00039	0.02494 ± 0.00016	0.00030 ± 0.00006	0.05009 ± 0.00099	−0.000010 ± 0.00004	3.36E−16	114.83%	2.0922	24.32 ± 5.06	20.79%

*Rejected data. P: % power of 60 W (60 W *(P/10) Synrad CO_2 laser); t: laser duration time; V: volt; %Rad: % radiogenic argon; R: $^{40}Ar^{*}/^{39}Ar$ (Ar^{*}: radiogenic argon); J value: 0.0064870 ± 0.000011 (1σ).

References

Akdeniz, N., Konak, N., 1979. Simav–Emet–Dursunbey–Demirci yörelerinin jeolojisi [Geology of the Simav–Emet–Dursunbey–Demirci areas]. Bulletin of Mineral Research and Exploration Institute of Turkey (unpublished) Report No: 6547.

Akgün, F., Kayseri, M.S., Akkiraz, S., 2007. Palaeoclimatic evolution and vegetational changes during the Late Oligocene–Miocene period in the Western and Central Anatolia (Turkey). Palaeogeogr. Palaeoclimatol. Palaeoecol. 253, 56–90.

Akyürek, B., Soysal, Y., 1983. Biga Yarımadası Güneyinin (Savaştepe–Kırkağaç–Ayvalık) Temel Jeolojik Özellikleri. Miner. Res. Explor. Bull. (Turkey) 95 (96), 1–13.

Aldanmaz, E., Pearce, J.A., Thirlwall, M.F., Mitchell, J.G., 2000. Petrogenetic evolution of late Cenozoic, post-collision volcanism in western Anatolia Turkey. J. Volcanol. Geotherm. Res. 102, 67–95.

Altunkaynak, Ş., Rogers, N.W., Kelley, S.P., 2010. Causes and effects of geochemical variations in late Cenozoic volcanism of the Foça volcanic centre, NW Anatolia, Turkey. Int. Geol. Rev. 52, 579–607.

Altunkaynak, Ş., Dilek, Y., Genç, Ş.C., Sunal, G., Gertisser, R., Furnes, H., Foland, K.A., Yang, J., 2012. Spatial, temporal and geochemical evolution of Oligo-Miocene granitoid magmatism in western Anatolia, Turkey. Gondwana Res. 21, 961–986.

Bingöl, E., Delaloye, M., Ataman, G., 1982. Granitic intrusions in Western Anatolia: a contribution to the geodynamic study of this area. Eclogae Geol. Helv. 75, 437–446.

Biryol, C.B., Beck, S.L., Zandt, G., Özacar, A.A., 2011. Segmented African lithosphere beneath the Anatolian region inferred from teleseismic P-wave tomography. Geophys. J. Int. 184, 1037–1057.

Boccaletti, M., Manetti, P., Peccerillo, A., 1974. The Balkanids as an instance of back-arc thrust belt: possible relation with the Hellenids. Geol. Soc. Am. Bull. 85, 1077–1084.

Borsi, J., Ferrara, G., Innocenti, F., Mazzuoli, R., 1972. Geochronology and petrology of recent volcanics in the eastern Aegean Sea (West Anatolia and Lesvos Iceland). Bull. Volcanol. 36, 473–496.

Bozkurt, E., 2000. Timing of extension on the Büyük Menderes Graben, Western Turkey and its tectonic implications. In: Bozkurt, E., Winchester, J.A., Piper, J.A.D. (Eds.), Tectonics and Magmatism in Turkey and the Surrounding Area. Journal of Geological Society of London 173, pp. 385—403–385—403.

Bozkurt, E., Park, R.G., 1994. Southern Menderes Massif—an incipient metamorphic core complex in western Anatolia, Turkey. J. Geol. Soc. Lond. 151, 213–216.

Bozkurt, E., Satır, M., Buğdaycıoğlu, Ç., 2011. Surprisingly young Rb/Sr ages from the Simav extensional detachment fault zone, northern Menderes Massif, Turkey. J. Geodyn. 52, 406–431.

Brun, J.-P., Faccenna, C., 2008. Exhumation of high-pressure rocks driven by slab rollback. Earth Planet. Sci. Lett. 272, 1–7.

Brun, J.-P., Sokoutis, D., 2012. 45 m.y. of Aegean crust and mantle flow driven by trench retreat. Geol. Soc. Am. 38, 815–818.

Candan, O., Çetinkaplan, M., Oberhänsli, R., Rimmelé, G., Akal, C., 2005. Alpine high-P/low-T metamorphism of the Afyon Zone and implications for the metamorphic evolution of Western Anatolia, Turkey. Lithos 84, 102–124.

Catlos, E.J., Çemen, İ., 2005. Monazite ages and rapid exhumation of the Menderes Massif, western Turkey. Int. J. Earth Sci. 94, 204–217.

Catlos, E.J., Baker, C.B., Sorensen, S.S., Çemen, İ., Hancer, M., 2008. Monazite geochronology, magmatism, and extensional dynamics within the Menderes Massif, western Turkey. Donald D Harrington Symposium on the Geology of the Aegean, Conf. Series: Earth and Environmental Science 2, p. 012013.

Catlos, E.J., Baker, J., Sorensen, S.S., Çemen, İ., Hançer, M., 2010. Geochemistry, geochronology, and cathodoluminescence imagery of the Salihli and Turgutlu granites (central Menderes Massif, western Turkey): Implications for Aegean tectonics. Tectonophysics 488, 110–130.

Çemen, İ., Göncüoğlu, C., Dirik, K., 1999. Structural evolution of the Tuzgölü Basin in Central Anatolia, Turkey. J. Geol. 107, 693–706.

Çemen, İ., Catlos, E.J., Göğüş, O., Özerdem, C., 2006. Postcollisional extensional tectonics and exhumation of the Menderes Massif in Western Anatolia extended terrane, Turkey. Geol. Soc. Am. Spec. Publ. 409, 353–379.

Çemen, İ., Ersoy, Y., Helvacı, C., Karaoglu, Ö., Oner, Z., 2012. Late Cenozoic Extensional Tectonics in Central and northern Menderes Massif, Western Turkey. International Earth Science Colloquium on the Aegean Region (IESCA-2012) Pre-Meeting Field Trip Guide, p. 71.

Çiftçi, N.B., Bozkurt, E., 2009. Pattern of normal faulting in the Gediz Graben, SW Turkey. Tectonophysics 473, 234–260.

Çiftçi, N.B., Bozkurt, E., 2010. Structural evolution of the Gediz Graben, SW Turkey: temporal and spatial variation of the graben basin. Basin Res. 22, 846–873.

Çoban, H., Karacık, Z., Ece, Ö.I., 2012. Source contamination and tectonomagmatic signals of overlapping Early to Middle Miocene orogenic magmas associated with shallow continental subduction and asthenospheric mantle flows in Western Anatolia: a record from Simav (Kütahya) region. Lithos 140–141, 119–141.

de Boorder, H., Spakman, W., White, S.H., Wortel, M.J.R., 1998. Late Cenozoic mineralization, orogenic collapse and slab detachment in the European Alpine Belt. Earth Planet. Sci. Lett. 164, 569–575.

Dinter, D.A., Royden, L., 1993. Late Cenozoic extension in northeastern Greece: Strymon Valley detachment system and Rhodope metamorphic core complex. Geology 21, 45–48.

Dönmez, M., Türkecan, A., Akçay, A.E., Hakyemez, Y., Sevin, D., 1998. İzmir ve kuzeyinin jeolojisi Tersiyer volkanizmasinin petrografik ve kimyasal özellikleri. [Geology of the northern part of İzmir and petrographic and chemical features of the Tertiary volcanism] Bulletin of Mineral Research and Exploration Institute of Turkey (unpublished) Report No:10181.

Emre, T., 1996. Gediz grabeninin jeolojisi ve tektoniği (Geology and tectonics of the Gediz graben). Turk. J. Earth Sci. 5, 171–185.

Emre, T., Sözbilir, H., 2005. Geology, geochemistry and geochronology of the Başlova andesite, eastern end of the Küçük Menderes Graben. Miner. Res. Explor. Inst. (MTA) Turk. Bull. 131, 1–19.

Ercan, T., Dinçel, A., Metin, S., Türkecan, A., Günay, A., 1978. Uşak yöresindeki Neojen havzalarının jeolojisi [Geology of the Neogene basins in Uşak region]. Bull. Geol. Soc. Turk. 21, 97–106 (in Turkish with English abstract).

Ercan, T., Satır, M., Kreuzer, H., Türkecan, A., Günay, E., Çevikbaş, A., Ateş, M., Can, B., 1985. Batı Anadolu Senozoyik volkanitlerine ait yeni kimyasal, izotopik ve radyometrik verilerin yorumu [Interpretation of new chemical, isotopic and radiometric data on Cenozoic volcanics of western Anatolia]. Bull. Geol. Soc. Turk. 28, 121–136.

Ercan, E., Satır, M., Sevin, D., Türkecan, A., 1996. Batı Anadolu'daki Tersiyer ve Kuvaterner yaşlı volkanik kayaçlarda yeni yapılan radyometrik yaş ölçümlerinin yorumu [Some new radiometric ages from Tertiary and Quaternary volcanic rocks from West Anatolia]. Miner. Res. Explor. Bull. (Turkey) 119, 103–112.

Erkül, F., Helvacı, C., Sözbilir, H., 2005. Stratigraphy and geochronology of the Early Miocene volcanic units in the Bigadiç Borate Basin, Western Turkey. Turk. J. Earth Sci. 14, 227–253.

Erkül, F., Erkül, S.T., Ersoy, E.Y., Karaoğlu, Ö., 2012. Peperites associated with ultrapotassic lava flows, Western Turkey. International Multidisciplinary Scientific GeoConference & EXPO. Surveying Geology & Mining Ecology Management (SGEM-2012), Albena, Bulgaria (Proceedings) vol. 1, pp. 233–240 (ISSN 1314/2704).

Ersoy, E.Y., Palmer, M.R., 2013. Eocene–Quaternary magmatic activity in the Aegean: implications for mantle metasomatism and magma genesis in an evolving orogeny. Lithos 180–181, 5–24.

Ersoy, E.Y., Helvacı, C., Bozkurt, E., Erkül, F., Sözbilir, H., 2005. Oligocene (?)–Lower Miocene olistostromal sedimentary sequence structurally above the Menderes Metamorphic Core Complex, Selendi Basin, western Anatolia and its tectonic implications. International Symposium on the Geodynamics of Eastern Mediterranean, 15–8 June 2005, İstanbul, Abstracts, p. 75.

Ersoy, Y., Helvacı, C., Sözbilir, H., Erkül, F., Bozkurt, E., 2008. A geochemical approach to Neogene–Quaternary volcanic activity of western Anatolia: an example of episodic bimodal volcanism within the Selendi Basin, Turkey. Chem. Geol. 255, 265–282.

Ersoy, E.Y., Helvacı, C., Sözbilir, H., 2010a. Tectono-stratigraphic evolution of the NE–SW-trending superimposed Selendi basin: implications for Late Cenozoic crustal extension in western Anatolia, Turkey. Tectonophysics 488, 210–232.

Ersoy, E.Y., Helvacı, C., Palmer, M.R., 2010b. Mantle source characteristics and melting models for the early–middle Miocene mafic volcanism in Western Anatolia: implications for enrichment processes of mantle lithosphere and origin of K-rich volcanism in post-collisional settings. J. Volcanol. Geotherm. Res. 198, 112–128.

Ersoy, E.Y., Helvacı, C., Palmer, M.R., 2011. Stratigraphic, structural and geochemical features of the NE–SW-trending Neogene volcano-sedimentary basins in western Anatolia: implications for associations of supradetachment and transtensional strike-slip basin formation in extensional tectonic setting. J. Asian Earth Sci. 41, 159–183.

Ersoy, E.Y., Helvacı, C., Palmer, M.R., 2012. Petrogenesis of the Neogene volcanic units in the NE–SW-trending basins in western Anatolia, Turkey. Contrib. Mineral. Petrol. 163, 379–401.

Genç, Ş.C., Yılmaz, Y., 2000. Aliağa dolaylarının jeolojisi ve genç tektoniğ (Geology and young tectonics of the Aliağa region). The Symposia on the Earthquake Possibility of Western Anatolia, İzmir, pp. 152–159.

Genç, Ş.C., Altunkaynak, Ş., Karacık, Z., Yılmaz, Y., Yazman, M., 2001. The Çubukludağ Graben, Karaburun peninsula: its tectonic significance in the Neogene geological evolution of the western Anatolia. Geodin. Acta 14, 45–55.

Gessner, K., Gallardo, L.A., Markwitz, V., Ring, U., Thomson, S.N., 2013. What caused the denudation of the Menderes Massif: review of crustal evolution, lithosphere structure, and dynamic topography in southwest Turkey. Gondwana Res. 24, 243–274.

Glodny, J., Hetzel, R., 2007. Precise U–Pb ages of syn-extensional Miocene intrusions in the central Menderes Massif, Western Turkey. Geol. Mag. 144, 235–246.

Gürer, Ö.F., Bozcu, M., Yılmaz, K., Yılmaz, Y., 2001. Neogene basin development around Söke–Kuş adası (western Anatolia) and its bearing on tectonic development of the Aegean region. Geodin. Acta 14, 57–69.

Gürer, Ö.F., Sarica-Filoreau, N., Özburan, M., Sangu, E., Doğan, B., 2009. Progressive development of the Büyük Menderes Graben based on new data, western Turkey. Geol. Mag. 146, 652–673.

Hasözbek, A., Akay, E., Erdoğan, B., Satır, M., Siebel, W., 2010. Early Miocene granite formation by detachment tectonics or not? A case study from the northern Menderes Massif (Western Turkey). J. Geodyn. 50, 67–80.

Helvacı, C., 1986. Stratigraphic and structural evolution of the Emet borate deposits, Western Anatolia. Dokuz Eylül University, Faculty of Engineering and Architecture, Research Papers, No: MM/JEO-86 AR 008.

Helvacı, C., 1995. Stratigraphy, mineralogy, and genesis of the Bigadiç borate deposits, Western Turkey. Econ. Geol. 90, 1237–1260.

Helvacı, C., Alonso, R.N., 2000. Borate deposits of Turkey and Argentina; a summary and geological comparison. Turk. J. Earth Sci. 24, 1–27.

Helvacı, C., Stamatakis, M., Zagouroğlou, C., Kanaris, J., 1993. Borate minerals and related authigenic silicates in northeastern Meditarranean Late Miocene continental basins. Explor. Min. Geol. 2 (2), 171–178.

Helvacı, C., Ersoy, E.Y., Sözbilir, H., Erkül, F., Sümer, Ö., Uzel, B., 2009. Geochemistry and $^{40}Ar/^{39}Ar$ geochronology of Miocene volcanic rocks from the Karaburun Peninsula: implications for amphibole-bearing lithospheric mantle source, Western Anatolia. J. Volcanol. Geotherm. Res. 185, 181–202.

Hetzel, R., Ring, U., Akal, C., Troesch, M., 1995. Miocene NNE-directed extensional unroofing in the Menderes Massif, southwestern Turkey. J. Geol. Soc. Lond. 152, 639–654.

İnci, U., 1984. Neogene oil shale deposits of Demirci and Burhaniye regions. 27th International Geological Congress, Abs vol. VII, pp. 13–16 (57).

İnci, U., 1991. Torbalı (İzmir) kuzeyindeki Miyosen tortul istifinin fasiyesi ve çökelme ortamları. Miner. Res. Explor. Bull. (Turkey) 112, 13–26.
İnci, U., 1998. Miocene synvolcanic alluvial sedimentation in lignite-bearing Soma Basin, western Turkey. Turk. J. Earth Sci. 7, 63–78.
İnci, U., 2002. Depositional evolution of Miocene coal successions in the Soma coalfield, western Turkey. Int. J. Coal Geol. 51, 1–29.
Innocenti, F., Agostini, S., Di Vincenzo, G., Doglioni, C., Manetti, P., Savaşçın, M.Y., Tonarini, S., 2005. Neogene and Quaternary volcanism in Western Anatolia: magma sources and geodynamic evolution. Mar. Geol. 221, 397–421.
Işık, V., Tekeli, O., 2001. Late orogenic crustal extension in the northern Menderes Massif (Western Turkey); evidence for metamorphic core complex formation. Int. J. Earth Sci. 89, 757–765.
Işık, V., Seyitoğlu, G., Çemen, İ., 2000. Ductile–brittle transition along the Alaşehir shear zone and its structural relationship with the Simav Detachment, Menderes Massif, western Turkey. Tectonophysics 374, 1–18.
Işık, V., Tekeli, O., Seyitoğlu, G., 2004. The $^{40}Ar/^{39}Ar$ age of extensional ductile deformation and granitoid intrusion in the northern Menderes core complex: implications for the initiation of extensional tectonics in western Turkey. J. Asian Earth Sci. 23, 555–566.
Jolivet, L., Brun, J.-P., 2010. Cenozoic geodynamic evolution of the Aegean. Int. J. Earth Sci. 99, 109–138.
Jolivet, L., et al., 2013. Aegean tectonics: strain localisation, slab tearing and trench retreat. Tectonophysics 597–598, 1–33.
Karacık, Z., Yılmaz, Y., Pearce, J.A., 2007. The Dikili–Çandarlı volcanics, western Turkey: magmatic interactions as recorded by petrographic and geochemical features. Turk. J. Earth Sci. 16, 493–522.
Karacık, Z., Genç, Ş.C., Gülmez, F., 2013. Petrochemical features of Miocene volcanism around the Çubukludağ graben and Karaburun peninsula, western Turkey: implications for crustal melting related silicic volcanism. J. Asian Earth Sci. 73, 199–217.
Karaoğlu, Ö., 2014. Tectonic controls on the Yamanlar volcano and Yuntdağı volcanic region, western Turkey: Implications for an incremental deformation. Journal of Volcanology and Geothermal Research 274, 16–33.
Karaoğlu, Ö., Helvacı, C., 2012. Structural evolution of the Uşak–Güre supra-detachment basin during Miocene extensional denudation in western Turkey. J. Geol. Soc. Lond. 169, 627–642.
Karaoğlu, Ö., Helvacı, C., Ersoy, E.Y., 2010. Petrogenesis and $^{40}Ar/^{39}Ar$ geochronology of the volcanic rocks of the Uşak–Güre basin, western Türkiye. Lithos 119, 193–210.
Kaya, O., 1981. Miocene reference section for the coastal parts of West Anatolia. Newsl. Stratigr. 10, 164–191.
Kaya, T., Geraads, D., Tuna, V., 2003. A new Middle Miocene mammalian fauna from Mordoğan (Western Turkey). Palaontol. Z. 77, 293–302.
Kaya, O., Ünay, E., Göktaş, F., Saraç, G., 2007. Early Miocene stratigraphy of Central West Anatolia, Turkey: implications for the tectonic evolution of the Eastern Aegean area. Geol. J. 42, 85–109.
Kissel, C., Laj, C., 1988. The tertiary geodynamical evolution of the Aegean arc: a paleomagnetic reconstruction. Tectonophysics 146, 183–201.
Kissel, C., Laj, C., Şengör, A.M.C., Poisson, A., 1987. Paleomagnetic evidence for rotation in opposite senses of adjacent blocks in Northeastern Aegea and western Anatolia. Geophys. Res. Lett. 14, 907–910.
Kissel, C., Laj, C., Poisson, A., Görür, N., 2003. Paleomagnetic reconstruction of the Cenozoic evolution of the Eastern Mediterranean. Tectonophysics 362, 199–217.
Koçyiğit, A., Yusufoğlu, H., Bozkurt, E., 1999. Evidence from the Gediz graben for episodic two-stage extension in Western Turkey. J. Geol. Soc. Lond. 156, 605–616.
Kondopoulou, D., Sen, S., Aidona, E., van Hinsbergen, D.J.J., Koufos, G., 2011. Rotation history of Chios Island, Greece since the Middle Miocene. J. Geodyn. 51, 327–338.
Le Pichon, X., Angelier, J., 1981. The Aegean Sea. Philos. Trans. R. Soc. Lond. A300, 357–372.
Lips, A.L.W., Cassard, D., Sözbilir, H., Yılmaz, H., Wijbrans, J.R., 2001. Multistage exhumation of the Menderes Massif, Western Anatolia (Turkey). Int. J. Earth Sci. 89, 781–792.
Ludwig, K.R., 2003. User's manual for Isoplot, v. 3.0, a geochronological tool kit for Microsoft Excel. Berkeley Geochronological Center, Berkeley, CA, Special, Publication no. 4.
Meulenkamp, J.E., Wortel, M.J.R., Van Wamel, W.A., Spakman, W., Hoogerduyn Strating, E., 1988. On the Hellenic subduction zone and the geodynamical evolution of Crete since the late Middle Miocene. Tectonophysics 146, 203–215.
Meulenkamp, J.E., Van der Zwaan, G.J., Van Wamel, W.A., 1994. On Late Miocene to Recent vertical motions in the Cretan segment of the Helennic arc. Tectonophysics 234, 53–72.
Okay, A.İ., Tüysüz, O., 1999. Tethyan sutures of northern Turkey. In: Durand, B., Jolivet, L., Hovarth, F., Séranne, M. (Eds.), The Mediterranean Basins: Tertiary Extension Within the Alpine Orogen. Journal of Geological Society of London 156, pp. 475–515.
Öner, Z., Dilek, Y., 2013. Supradetachment basin evolution during continental extension: the Aegean province of western Anatolia, Turkey. Geol. Soc. Am. Bull. 123, 2115–2141.
Özkaymak, Ç., Sözbilir, H., Uzel, B., 2013. Neogene–Quaternary evolution of the Manisa Basin: evidence for variation in the stress pattern of the İzmir–Balıkesir Transfer Zone, western Anatolia. J. Geodyn. 65, 117–135.
Pe-Piper, G., Piper, D.J.W., 2007. Late Miocene igneous rocks of Samos: the role of tectonism in petrogenesis in the southeastern Aegean. Geol. Soc. Lond., Spec. Publ. 291, 75–97.
Pe-Piper, G., Piper, D.J.W., Matarangas, D., 2002. Regional implications of geochemistry and style of emplacement of Miocene I-type diorite and granite, Delos, Cyclades, Greece. Lithos 60, 47–66.
Plunder, A., Agard, P., Chopin, C., Okay, A.I., 2013. Geodynamics of the Tavşanlı zone, western Turkey: insights into subduction/obduction processes. Tectonophysics 608, 884–903.
Prelević, D., Akal, C., Foley, F., Romer, R.L., Stracke, A., van den Bogaard, P., 2012. Ultrapotassic mafic rocks as geochemical proxies for post-collisional dynamics of orogenic lithospheric mantle: the case of southwestern Anatolia, Turkey. J. Petrol. 53, 1019–1055.
Purvis, M., Robertson, A., Pringle, M., 2005. $^{40}Ar–^{39}Ar$ dating of biotite and sanidine in tuffaceous sediments and related intrusive rocks: implications for the early Miocene evolution of the Gördes and Selendi basins, W Turkey. Geodin. Acta 18, 239–253.
Renne, P.R., Swisher, C.C., Deino, A.L., Karner, D.B., Owens, T.L., DePaolo, D.J., 1998. Intercalibration of standards, absolute ages, and uncertainties in $^{40}Ar/^{39}Ar$ dating. Chem. Geol. 145, 117–152.
Ricou, L.-E., Burg, J.-P., Godfriaux, I., Ivanov, Z., 1998. Rhodope and Vardar: the metamorphic and the olistostromic paired belts related to the Cretaceous subduction under Europe. Geodin. Acta 11, 285–309.
Rimmelé, G., Oberhänsli, R., Goffé, B., Jolivet, L., Candan, O., Çetinkaplan, M., 2003. First evidence of high-pressure metamorphism in the "Cover Series" of the southern Menderes Massif. Tectonic and metamorphic implications for the evolution of SW Turkey. Lithos 71, 19–46.
Ring, U., Collins, A.S., 2005. U–Pb SIMS dating of synkinematic granites: timing of core-complex formation in the northern Anatolide belt of western Turkey. J. Geol. Soc. Lond. 162, 289–298.
Ring, U., Layer, P.W., Reischmann, T., 2001. Miocene high-pressure metamorphism in the Cyclades and Crete, Aegean Sea, Greece: evidence for large-magnitude displacement on the Cretan detachment. Geol. Soc. Am. 29, 395–398.
Ring, U., Johnson, C., Hetzel, R., Gessner, K., 2003. Tectonic Denudation of a Late Cretaceous–Tertiary collisional belt: regionally symmetric cooling patterns and their relation to extensional faults in the Anatolide belt of Western Turkey. Geol. Mag. 140, 421–441.
Ring, U., Glodny, J., Will, T., Thomson, S., 2010. The Hellenic subduction system: high-pressure metamorphism, exhumation, normal faulting, and large-scale extension. Annu. Rev. Earth Planet. Sci. 38, 45–76.
Schellart, W.P., Jessell, M.W., Lister, G.S., 2003. Asymmetric deformation in the backarc region of the Kuril arc, northwest Pacific: new insights from analogue modeling. Tectonics 22, 1047. http://dx.doi.org/10.1029/2002TC001473.
Şen, Ş., Seyitoğlu, G., 2009. Magnetostratigraphy of early–middle Miocene deposits from east–west trending Alaşehir and Büyük Menderes grabens in western Turkey, and its tectonic implications. Geol. Soc. Lond. Spec. Publ. 311, 321–342.
Şengör, A.M.C., Yılmaz, Y., 1981. Tethyan evolution of Turkey: a plate tectonic approach. Tectonophysics 75, 181–241.
Şengör, A.M.C., Görür, N., Şaroğlu, 1985. Strike-slip faulting and related basin formation in zones of tectonic escape: Turkey as a case study. In: Biddle, K.T., Christie-Blick, N. (Eds.), Strike-slip Faulting and Basin Formation and Sedimentation. Society of Economic Paleontologists and Mineralogists Special Publication 37, pp. 227–264.
Seyitoğlu, G., 1997a. Late Cenozoic tectono-sedimentary development of the Selendi and Uşak–Güre basins: a contribution to the discussion on the development of east–west and north trending basins in Western Turkey. Geol. Mag. 134, 163–175.
Seyitoğlu, G., 1997b. The Simav graben: an example of young E–W trending structures in the late Cenozoic extensional system of Western Turkey. Turk. J. Earth Sci. 6, 135–141.
Seyitoğlu, G., Scott, B.C., 1994. Late Cenozoic basin development in west Turkey: Gördes basin tectonics and sedimentation. Newsl. Stratigr. 131, 133–142.
Seyitoğlu, G., Scott, B.C., Rundle, C.C., 1992. Timing of Cenozoic extensional tectonics in west Turkey. J. Geol. Soc. 149, 533–538.
Seyitoğlu, G., Anderson, D., Nowell, G., Scott, B., 1997. The evolution from Miocene potassic to Quaternary sodic magmatism in Western Turkey: implications for enrichment processes in the lithospheric mantle. J. Volcanol. Geotherm. Res. 76, 127–147.
Seyitoglu, G., Tekeli, O., Çemen, İ., Şen, S., Işık, V., 2002. The role of the flexural rotation/rolling hinge model in the tectonic evolution of the Alaşehir graben, western Turkey. Geol. Mag. 139, 15–26.
Seyitoğlu, G., Işık, V., Çemen, İ., 2004. Complete Tertiary exhumation history of the Menderes massif, western Turkey: an alternative working hypothesis. Terra Nova 16, 358–364.
Seyitoğlu, G., Alçiçek, M.C., Işık, V., Alçiçek, H., Mayda, S., Varol, B., Yılmaz, İ., Esat, K., 2009. The stratigraphical position of Kemiklitepe fossil locality (Uşak–Eşme) revisited: implications for the Late Cenozoic sedimentary basin development and extensional tectonics in Western Turkey. N. Jb. Geol. Paläont. 251, 1–15.
Siyako, M., Bürkan, K.A., Okay, A.İ., 1989. Biga ve Gelibolu yarımadalarının Tersiyer jeolojisi ve hidrokarbon olanaklar (Tertiary geology and hydrocarbon potential of the Biga and Gelibolu peninsulas). TAPG Bulletin 1/3, 183–199. (in Turkish with English abstract).
Sözbilir, H., 2002. Geometry and origin of folding in the Neogene sediments of the Gediz Graben, western Anatolia, Turkey. Geodin. Acta 15, 277–288.
Sözbilir, H., 2005. Oligo-Miocene extension in the Lycian orogen: evidence from the Lycian molasse basin, SW Turkey. Geodin. Acta 18, 257–284.
Sözbilir, H., İnci, U., Erkül, F., Sümer, Ö., 2003. An active intermittent transform zone accomodating N–S extension in western Anatolia and its relation to the North Anatolian Fault System. International Workshop on the North Anatolian, East Anatolian and Dead Sea Fault Systems. Middle East Technical University, Cultural Convention Center, Ankara, Turkey, p. 87 (Abstracts).
Sözbilir, H., Sarı, B., Uzel, B., Sümer, Ö., Akkiraz, S., 2011. Tectonic implications of transtensional supradetachment basin development in an extension-parallel transfer zone: the Kocacay Basin, western Anatolia, Turkey. Basin Res. 23, 423–448.
Spakman, W., Wortel, M.R.J., Vlaar, N.J., 1988. The Hellenic Subduction Zone: a tomographic image and its geodynamic implications. Geophys. Res. Lett. 15, 60–63.
Sümer, Ö., İnci, U., Sözbilir, H., 2013. Tectonic evolution of the Söke Basin: extension-dominated transtensional basin formation in western part of the Büyük Menderes Graben, Western Anatolia, Turkey. J. Geodyn. 65, 148–175.

Thomson, S.N., Ring, U., 2006. Thermochronologic evaluation of postcollision extension in the Anatolide orogen, western Turkey. Tectonics 25, TC3005.
Türkecan, A., Ercan, T., Sevin, D., 1998. Karaburun Yarımadası'nın Neojen volkanizması (Neogene volcanism in Karaburun Peninsula). Report no: 10185, General Directorate of Mineral research and Exploration, Ankara.
Uzel, B., Sözbilir, H., 2008. A first record of a strike-slip basin in western Anatolia and its tectonic implication: the Cumaovası Basin. Turk. J. Earth Sci. 17, 559–591.
Uzel, B., Sözbilir, H., Özkaymak, Ç., 2012. Neotectonic evolution of an actively growing superimposed basin in western Anatolia: the inner bay of İzmir, Turkey. Turk. J. Earth Sci. 21, 439–471.
Uzel, B., Sözbilir, H., Özkaymak, Ç., Kaymakçı, N., Langereis, C.G., 2013. Structural evidence for strike-slip deformation in the İzmir–Balıkesir transfer zone and consequences for late Cenozoic evolution of western Anatolia (Turkey). J. Geodyn. 65, 94–116.
van Hinsbergen, D.J.J., 2010. A key extensional metamorphic complex reviewed and restored: the Menderes Massif of western Turkey. Earth Sci. Rev. 102, 60–76.
van Hinsbergen, D.J.J., Schmid, S.M., 2012. Map view restoration of Aegean–West Anatolian accretion and extension since the Eocene. Tectonics 31, TC5005.
van Hinsbergen, D.J.J., Hafkenscheid, E., Spakman, W., Meulenkamp, J.E., Wortel, R., 2005. Nappe stacking resulting from subduction of oceanic and continental lithosphere below Greece. Geology 33, 325–328.
van Hinsbergen, D.J.J., Dekkers, M.J., Bozkurt, E., Koopman, M., 2010a. Exhumation with a twist: paleomagnetic constraints on the evolution of the Menderes metamorphic core complex, western Turkey. Tectonics 29, TC3009.
van Hinsbergen, D.J.J., Kaymakçı, N., Spakman, W., Torsvik, T.H., 2010b. Reconciling the geological history of western Turkey with plate circuits and mantle tomography. Earth Planet. Sci. Lett. 297, 674–686.
Walcott, C.R., White, S.H., 1998. Constraints on the kinematics of post-orogenic extension imposed by stretching lineations in the Aegean region. Tectonophysics 298, 155–175.
Yiğitbaş, E., Elmas, A., Yılmaz, Y., 1999. Pre-Cenozoic tectono-stratigraphic components of theWestern Pontides and their geological evolution. Geol. J. 34, 55–74.
Yılmaz, Y., Genç, Ş.C., Gürer, F., Bozcu, M., Yılmaz, K., Karacık, Z., Altunkaynak, Ş., Elmas, A., 2000. When did the Western Anatolian grabens begin to develop? In: Bozkurt, E., Winchester, J.A., Piper, J.A.D. (Eds.), Tectonics and Magmatism in Turkey and the Surrounding Area. Journal of Geological Society of London 173, pp. 131–162.